Two-Color Picosecond Time-Resolved (2 + 1') Resonance-Enhanced Multiphoton Ionization Photoelectron Spectroscopy on the B1E'' and C' 1A1' States of Ammonia

ARTICLE *in* THE JOURNAL OF PHYSICAL CHEMISTRY · APRIL 1995

Impact Factor: 2.78 · DOI: 10.1021/j100006a009

3 AUTHORS, INCLUDING:

Wybren J Buma
University of Amsterdam
184 PUBLICATIONS **2,411** CITATIONS
SEE PROFILE

Cornelis A de Lange
VU University Amsterdam
232 PUBLICATIONS **2,969** CITATIONS
SEE PROFILE

Two-Color Picosecond Time-Resolved (2 + 1′) Resonance-Enhanced Multiphoton Ionization Photoelectron Spectroscopy on the $\tilde{B}$ $^1E''$ and $\tilde{C}'$ $^1A_1'$ States of Ammonia

M. R. Dobber, W. J. Buma, and C. A. de Lange*

Laboratory for Physical Chemistry, University of Amsterdam, Nieuwe Achtergracht 127, 1018 WS Amsterdam, The Netherlands

Received: June 29, 1994; In Final Form: September 6, 1994[⊗]

The picosecond predissociation dynamics of vibronic levels of the $\tilde{B}$ and $\tilde{C}'$ Rydberg states of ammonia have been investigated in real time by (2 + 1′) two-color pump−probe ionization in combination with photoelectron spectroscopy. The picosecond real-time results are in reasonable agreement with the results obtained from indirect methods using nanosecond excitation. These indirect methods include investigations of the peak intensities and the natural line widths of the rotational lines in the excitation spectra. The photoelectron spectra obtained for (2 + 1) ionization *via* the $\tilde{B}$ state in NH_3 and ND_3 are interpreted and shown to allow for an accurate determination of hitherto unknown vibrational frequencies in the ground state of NH_3^+ (ND_3^+). For the ν_1 symmetric stretch a frequency of 0.404 ± 0.007 eV (0.304 ± 0.007 eV) is found, while the frequency of the ν_4 asymmetric bend vibration has been established as 0.197 ± 0.007 eV (0.141 ± 0.007 eV). The hydrogen atom fragment, which results from the predissociation of the $\tilde{B}$ and $\tilde{C}'$ Rydberg states, has been detected in a two-color pump−probe experiment using nanosecond excitation.

I. Introduction

The excited Rydberg states of the ammonia molecule show dynamical decay behavior on a time scale which ranges from femtoseconds to nanoseconds. Numerous studies on the spectroscopic properties as well as on the decay characteristics of the individual rotational levels associated with these excited Rydberg states have made the ammonia molecule a benchmark system for small polyatomic molecules.

Ammonia in its electronic ground state has a $...(1e)^4(3a_1)^2$ $\tilde{X}$ $^1A_1$ configuration in the C_{3v} point group and a pyramidal geometry. Due to inversion doubling, the ground state is split into two components separated by 0.793 cm^{-1} in NH_3 and 0.053 cm^{-1} in ND_3.[1,2] These components are usually designated as $^1A_1'$ and $^1A_2''$ in the D_{3h} symmetry group. The molecule has four vibrational modes: the $\nu_1(a_1')$ symmetric stretch, the $\nu_2(a_2'')$ out-of-plane bend, and two doubly degenerate vibrations, the $\nu_3(e')$ asymmetric stretch and the $\nu_4(e')$ asymmetric bend. The ground-state configuration in D_{3h} is given by $...(1e')^4(1a_2'')^2$ $\tilde{X}$ $^1A_1'$. Excitation of an electron from the $1a_2''$ highest occupied lone-pair orbital, centered on the nitrogen atom and responsible for the pyramidal geometry of the ground state, leads to planar geometries for all excited Rydberg states that result from such transitions. The spectroscopic properties of the molecule are consequently in general described in the D_{3h} point group. As a result of the large geometry change, the transitions to the Rydberg states show long progressions in the ν_2' out-of-plane bending mode.

The first Rydberg state ($\tilde{A}$ $^1A_2''$) results from the $1a_2'' \rightarrow 3sa_1'$ excitation and has been studied extensively. Investigations of the contours and the natural line widths of the rotational lines have shown that the rotational levels associated with the ν_2' vibrational members are short lived, with typical natural lifetimes of 100 fs in NH_3 and 5 ps in ND_3.[3−16] These short lifetimes are a consequence of a predissociation process, which yields H and NH_2 fragments. The exact details of this predissociation process in the $\tilde{A}$ state have been studied extensively.[4,7,10,17−24] Investigations of the spectroscopic properties and the line widths of the individual rotational lines are severely hampered by the lack of rotational resolution for most $\tilde{A}(\nu_2')$ vibrational members as a result of the short natural lifetimes. In a resonance Raman study rotational resolution has been obtained, however, and from the line widths the femtosecond lifetimes of individual rotational levels could be established.[11,15,25] The $\tilde{A}$ state has attracted interest not only because of its own spectroscopic and dynamic properties but certainly also because of the profound influence it has on the predissociation processes occurring in higher-lying Rydberg states.[26−29]

It is by now well established that excitation of a $1a_2''$ electron to the 3p Rydberg orbital results in the degenerate $\tilde{B}$ $^1E''$ Rydberg state ($1a_2'' \rightarrow 3p_{x,y}$ e′) and the $\tilde{C}'$ $^1A_1'$ Rydberg state ($1a_2'' \rightarrow 3p_z$ a_2'').[4,28,30−33] Rotationally resolved transitions to the $\tilde{B}$ (ν_2') vibrational members have been examined in vacuum absorption measurements[3,4,34] as well as in (2 + 1)[29,35−40] and (3 + 1)[26,33,41−43] resonance-enhanced multiphoton ionization (REMPI) studies, whereas the $\tilde{C}'$ (ν_2') levels have, as yet, only been observed by (2 + 1)[27,35,36,44,45] and (3 + 1)[26,31−33,41−43] REMPI. These studies have resulted in a vast amount of spectroscopic information on the $\tilde{B}$ (ν_2') and $\tilde{C}'$ (ν_2') Rydberg states. Comparison of the experimentally observed intensities of rotational transitions with theoretically predicted values[26,41] and accurate sub-Doppler natural line width measurements[27,29] have enabled an indirect determination of the dynamical predissociation behavior in these Rydberg states.

REMPI in combination with photoelectron spectroscopy (PES) can provide valuable additional information on the ionization process as well as on the spectroscopic and dynamical properties of the excited state under investigation. When REMPI−PES is combined with a picosecond or femtosecond excitation source, it becomes possible to investigate the dynamical processes occurring in these states *in real time*. In the present study we have used this combination to measure directly the natural lifetimes of rotational levels associated with the $\tilde{B}$ (ν_2') and $\tilde{C}'$ (ν_2') vibrational members of ammonia, which are excited and ionized in a (2 + 1′) REMPI process using a picosecond excitation source.

[⊗] Abstract published in *Advance ACS Abstracts*, January 15, 1995.

0022-3654/95/2099-1671$09.00/0

The outline of the present paper is as follows. In section II the experimental details of the picosecond and nanosecond excitation sources will be given. It will be shown that picosecond excitation in combination with photoelectron spectroscopy provides the possibility to perform background-free real-time pump−probe spectroscopy of highly excited molecular states. Subsequently, the (2 + 1) excitation spectra of the $\tilde{B}$ (v_2') and $\tilde{C}'$ (v_2') vibrational members in NH_3 and ND_3, as obtained with nanosecond and picosecond excitation sources, will be discussed (section III.A). The comparison of the intensities of rotational transitions in the experimental excitation spectra with theoretically predicted rotational contour simulations enables an indirect investigation of the rotational-level-dependent predissociation dynamics. The same type of information can be obtained from the natural line widths of the individual rotational lines in the excitation spectra (section III.B). The results from these indirect methods will be discussed. In section III.C the photoelectron spectra obtained for (2 + 1) excitation *via* the $\tilde{B}$ (v_2') and $\tilde{C}'$ (v_2') vibrational members are described and the $\tilde{B}$ (v_2') photoelectron spectra in NH_3 and ND_3 will be discussed in detail. The latter photoelectron spectra allow for the determination of previously unknown vibrational frequencies in the ground state of the NH_3^+ and ND_3^+ ions. In section III.D the results from the real-time lifetime measurements of rotational levels associated with the $\tilde{B}$ (v_2') and $\tilde{C}'$ (v_2') vibrational members in NH_3 and ND_3 are presented. These results are subsequently compared to the results from the above, indirect, methods in section III.E. Finally, the fragmentation mechanisms of the $\tilde{B}$ (v_2') and $\tilde{C}'$ (v_2') states are discussed in section III.F, and it will be shown that the detection of the hydrogen atom predissociation fragment from the Rydberg states allows for the observation of the predissociation decay channel, competing with the ionization channel.

II. Experimental Details

II.A. Experimental Setup. In the present study picosecond and nanosecond laser systems are used in combination with a "magnetic bottle" electron spectrometer. The "magnetic bottle" electron spectrometer setup has been described previously.[46−48] Briefly, the laser light is focused into the ionization region by means of a plano-convex quartz lens with a focal length of 25 mm. A similar lens is located on the other side of the spectrometer. This lens provides the possibility to focus a second laser beam into the ionization region and thus to perform two-color experiments. A strongly diverging magnetic field parallellizes 50% of the electrons produced in a laser shot, which are subsequently spatially separated according to their kinetic energies in a 50 cm long flight tube. After detection by a pair of microchannel plates the signal is amplified by a home-built preamplifier and stored in a transient digitizer, which is connected to a microcomputer for further analysis. A photoelectron spectrum is built up in the computer by increasing in steps the retarding voltage on a grid in the flight tube and transforming each time only the high-resolution part of the time-of-flight spectrum. By this technique a 15 meV resolution (fwhm) can be obtained at all electron kinetic energies in the present experiments. The spectrometer is calibrated using the lower spin−orbit ionic states of atomic krypton. The laser pulse peak power is kept as low as possible in order to avoid space−charge effects in the focal region.

Apart from kinetic-energy-resolved electron detection the "magnetic bottle" spectrometer also allows for mass-resolved ion detection by application of appropriate voltages to two grids at opposite sides of the ionization region.[47,48] The detection efficiency is, however, lower than for electron detection.

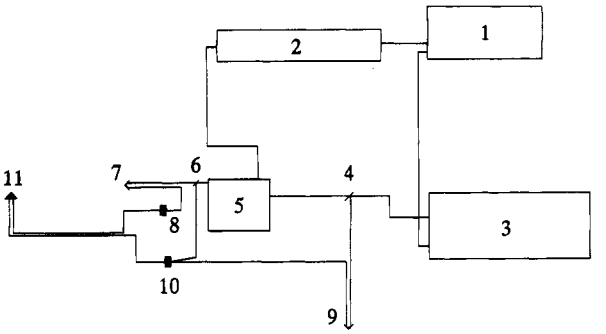

Figure 1. Schematic diagram of the experimental picosecond setup. The figure contains one dye laser and one dye amplifier, but a total of three dye lasers and two dye amplifiers are available for the experiments: (1) Nd:YLF pump laser; (2) synchronously pumped picosecond or hybridly mode-locked femtosecond dye laser; (3) Nd:YLF regenerative amplifier; (4) 85/15 beamsplitter; (5) dye amplifier; (6) 20/80 beamsplitter; (7) computer-controlled delay line; (8) KDP frequency-doubling crystal; (9) fixed delay line; (10) KDP crystal used for frequency doubling or mixing; (11) "magnetic bottle" electron spectrometer.

NH_3 gas (99.96 vol %, Messer Griesheim) and ND_3 gas (99.5 atom % D, MSD) were effusively introduced into the spectrometer. Typical pressures were 1×10^{-4} mbar in the ionization region and 1×10^{-6} mbar in the flight tube with a system background pressure of 2×10^{-7} mbar.

Parts of the picosecond laser system have also been described previously.[47] A schematic overview of the picosecond setup used in the present experiments is shown in Figure 1. A CW mode-locked Nd:YLF laser (Coherent Antares 76) produces 18 W average output power at 1053 nm in pulses with a temporal width of 50 ps at a repetition rate of 76 MHz. This beam is frequency doubled in a 12 mm long temperature-tuned LBO crystal. The maximum average output at 526.5 nm is 5 W, but during the experiments the crystal is slightly detuned from the focus to produce 2.5 W output in pulses with a temporal width of 35 ps. The 526.5 nm beam is used to pump synchronously one or two dye lasers (one or two Coherent CR-590 or one Coherent Satori 774). In most of our experiments on ammonia only one dye laser has been used, either the CR-590 picosecond dye laser or the Satori femtosecond dye laser, but in a few cases two CR-590 dye lasers have been employed simultaneously (see section III). The CR-590 dye lasers are operated on rhodamine 6G dissolved in ethylene glycol and have extended cavities, which are matched to the cavity length of the Nd:YLF pump laser. Computer-controlled wavelength selection in the range 560−640 nm on each of these dye lasers is possible by rotating a three-plate birefringent filter using an encoded dc motor. Each CR-590 dye laser is pumped by 1 W of 526.5 nm pump power, producing about 350 mW average output power in near-transform limited pulses with a temporal width of about 3 ps and a spectral width of about 5 cm^{-1}. The autocorrelation trace of the CR-590 dye lasers shows a near-Gaussian profile. The Satori femtosecond dye laser is a hybridly mode-locked laser which is operated on rhodamine 6G as the gain dye and DODCI as the saturable absorber. It is pumped by 2 W of 526.5 nm pump power and produces 250 mW average output power in the wavelength range 595−610 nm in near-transform limited pulses with a temporal width of 200 fs and a spectral width of 75 cm^{-1}. Wavelength selection is achieved by rotating a one-plate birefringent filter. To maintain the short temporal width of the pulses over long periods of time, the cavity length is actively stabilized. The femtosecond dye laser autocorrelation trace is also near-Gaussian.

In order to achieve amplification of the dye laser pulses from either the CR-590 or Satori 774 dye laser, 700 mW of the

remaining infrared beam from the Nd:YLF pump laser is seeded into a Nd:YLF regenerative amplifier (Continuum RGA 47-30) operating at a repetition rate of 30 Hz, which consists of an unstable resonator and a double-pass amplifier. The 1053 nm output with a temporal width of 50 ps is frequency doubled in a 10 mm long angle-tuned KD*P crystal. The output energy of the 526.5 nm pulses (temporal width 35 ps, near-Gaussian autocorrelation trace) can be adjusted by varying the voltage on the flashlamps of the double-pass amplifier stage and is maximally 10 mJ/pulse. The dye laser pulses are amplified using the output of the regenerative amplifier in a three-stage picosecond tunable dye amplifier (Continuum PTA 60). The three stages are all pumped longitudinally for maximum amplification. By splitting the regenerative amplifier output using a 50/50 beamsplitter, the two CR-590 dye lasers can be amplified separately in two different PTAs. In the present study the PTAs are operated on rhodamine 6G, rhodamine 101, or sulforhodamine 640 dissolved in methanol. Due to the solvent, the dye gain curve of the individual dyes is restricted to about 20 nm. In the case of the 3 ps dye laser pulses of the CR-590 dye lasers, the temporal width of the input dye laser pulses is maintained throughout the amplification process, whereas the femtosecond pulses of the Satori 774 dye laser are somewhat broadened to about 250 fs. The maximum output energy per pulse is 0.5 mJ. The short pump pulses from the regenerative amplifier guarantee an amplified spontaneous emission contribution of less than 1%.

For the real-time picosecond experiments described in this study both a pump and a probe pulse are required, preferably of different wavelengths, as will become clear later. The output of one of the PTAs is directed through a retroreflector mounted on a translational stage, which is driven by a computer-controlled stepper motor enabling a maximum delay of 800 ps. This beam is subsequently frequency-doubled in an angle-tuned KDP crystal, which is controlled by a dc motor with encoder. The resulting UV beam is used as the pump beam to achieve excitation. Different types of beams can be used as probe beams. In our experiments on ammonia each possible probe beam enables a different kind of experiment, as will become clear below and in section III. In principle, the same beam might be used to serve as both the pump and the probe beam, but this option does not take full advantage of the possibilities offered by the present setup (*vide infra*). A second possibility is to frequency-double the output of the second PTA in a second angle-tuned KDP crystal and employ the resulting UV beam as the probe beam. This has been done occasionally in the present study, *e.g.*, to observe the hydrogen atom, which results from predissociation of the $\tilde{B}$ and $\tilde{C}'$ Rydberg states of ammonia (see section III). Such a scheme results in a time resolution of about 4 ps. A third possibility is to use only one dye laser and one PTA and to split the output of the regenerative amplifier with a 85/15 beamsplitter. The 85% part is now used to pump the PTA to obtain the pump beam, while the remaining 15% is frequency-doubled in a KDP crystal yielding a 263.3 nm UV pulse which serves as the probe beam. In this case the time resolution is limited by the temporal width of the 263.3 nm probe pulse, *i.e.*, 30 ps. This option has been used to record (2 + 1′) picosecond excitation spectra of the $\tilde{B}$ and $\tilde{C}'$ Rydberg states of ammonia, for which the probe beam has a fixed time delay with respect to the pump beam (see section III). The last and, in the present experiments, mainly used option is to split in the above scheme, *i.e.*, a 85/15 partitioning of the output of the regenerative amplifier, also the PTA output with a 20/80 beamsplitter. The 20% beam provides the pump beam, whereas the remainder is frequency-mixed in a KDP crystal with the 15% part of the 526.5 nm beam from the regenerative amplifier. The resulting pulse has an energy of $\hbar\omega_{PTA} + \hbar\omega_{526.5}$ and a temporal width of about 4 ps. The overall time resolution is found to be about 5 ps. Mixing the 250 fs amplified pulse with the regenerative amplifier output produces pulses with a temporal width of about 2.5 ps, thus showing considerable temporal broadening in the mixing process. The overall time resolution is in this case 2.5 ps. The time delay between the pump and the probe laser pulses can be varied by repositioning the retroreflector in the pump beam path. The timing of both pulses is checked with a fast photodiode. Since this timing is of crucial importance, both the pump and probe beams enter the "magnetic bottle" spectrometer through the same lens on one side of the spectrometer.

The nanosecond laser system has been described previously as well.[47,48] A XeCl excimer laser (Lumonics HyperEx-460, 30 Hz repetition rate, temporal pulse width 10 ns, 200 mJ/pulse) pumps a dye laser (Lumonics HyperDye-500), whose output is subsequently frequency-doubled in a unit which is operated with an angle-tuned KD*P crystal (Lumonics HyperTrak-1000). The resulting UV pulses have a spectral width of about 0.15 cm^{-1}. In some experiments in which nanosecond excitation is used two dye lasers have been employed simultaneously. To this purpose, the pump beam is split using a 60/40 beamsplitter. The 40% beam is used to pump the first dye laser as described above. The remaining 60% pumps a second dye laser (Lumonics HyperDye-300) operating on coumarin 480. The dye laser output is frequency-doubled in a second frequency-doubling unit (INRAD II autotracker), which uses an angle-tuned BBO crystal. As the timing between the two UV pulses is not as critical as in the picosecond experiments, the two beams in these experiments enter the spectrometer from opposite sides.

II.B. Real-Time Picosecond Pump−Probe Experiments. In the present study the picosecond laser system is used to perform time-resolved experiments on highly excited molecular Rydberg states of ammonia. In this scheme a pump laser pulse excites the molecule from the ground state to the excited state of interest in a two-photon absorption process. A second laser pulse, the probe pulse, subsequently ionizes the molecule in a one-photon absorption step. By varying the time delay between the pump and probe pulses, it is possible to monitor in real time the excited-state population, which may be depleted by both radiative fluorescence processes and nonradiative processes such as (pre)dissociation. Apart from the ionization by such a (2 + 1′) ionization process, a certain number of molecules will also be ionized by only the pump beam, *i.e.*, a (2 + 1) ionization process. The latter process produces a contribution to the signal which is independent of the delay time. The use of the "magnetic bottle" electron spectrometer has the important advantage that these two processes can easily be separated. When ionization occurs by the (2 + 1) process, the photoelectron kinetic energies are given by $E_{kin} = 3h\nu - IE$, while (2 + 1′) ionization gives rise to photoelectrons with kinetic energies of $E_{kin} = 2h\nu + h\nu' - IE$, in which IE is an arbitrary ionization energy. If the difference in the energies of the two colors ($h\nu - h\nu'$) is large enough, it is possible to distinguish between the two processes. This is visualized in Figure 2, which shows the electron time-of-flight spectra when only the pump beam is present (Figure 2a) and when both pump and probe beams are present (Figure 2b). The observation that the electrons from both processes arrive at different times at the detector allows us to obtain background-free (2 + 1′) wavelength spectra and to study the temporal behavior of the (2 + 1′) signal in real time by varying the delay time between pump and probe pulses. Such background-free spectroscopy using the (2 + 1′) ionization

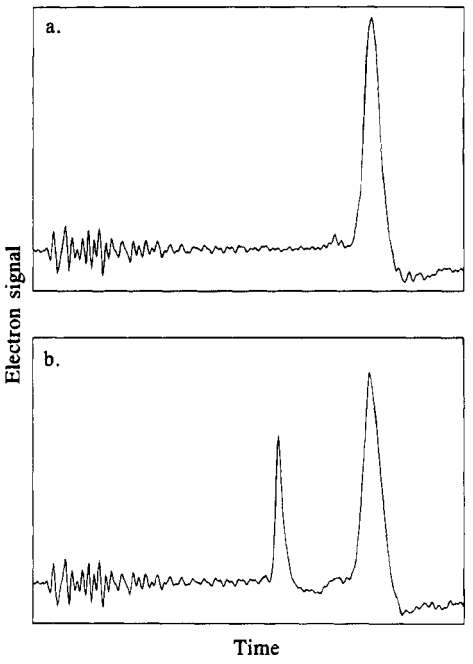

Figure 2. Photoelectron time-of-flight spectra obtained with one color ($h\nu$ = 32 637 cm^{-1}, Figure 2a), showing the (2 + 1) ionization signal, and with two different colors (Figure 2b) for excitation ($h\nu$ = 32 637 cm^{-1}, pump beam) and subsequent ionization ($h\nu'$ = 35 312 cm^{-1}, probe beam), showing the (2 + 1) one-color ionization signal to the right, as well as the (2 + 1′) two-color ionization signal to the left.

scheme described above would clearly not be possible if (mass-resolved) ion detection would have been used.

A typical decay trace is a convolution of the system response, which is the cross correlation of the UV pump and UV probe laser pulses, with a (multi)exponential decay. The signal increases to a maximum value following the system response and subsequently decreases exponentially to zero. The system response cannot be measured in a simple way and may be expected to vary from day to day, although we have found it to be constant for a time period of several hours. System responses are typically never exactly described by analytical functions. In the analysis of the decay traces in the present study it turned out that excellent fits could be obtained when a Gaussian profile was assumed for the system response. In a complementary experiment to the scheme described above it is also possible to use the probe laser pulse to ionize a (pre)dissociation fragment. The decay trace will then show an increase to a maximum value with comparable temporal behavior as in the scheme described above.

The time resolution in our experiments is limited on the low side by the system response. The approximate widths (fwhm) of system responses for different combinations of pump and probe pulses have been given above. On the high side the time window is limited by the length of the translational stage, which is 12 cm. The temporal window of the present study is thus 2.5−800 ps.

III. Results and Discussion

III.A. Excitation Spectra of Ammonia $\tilde{B}$ and $\tilde{C}'$ States. The $\tilde{B}$ and $\tilde{C}'$ Rydberg states of ammonia, which are investigated in the present study, have been examined previously using one-[3,4,34], two-[27,29,35−40,44,45] and three-photon[26,31−33,41−43] excitation. Due to the geometry change from pyramidal in the ground state to planar in the excited states, the excitation spectra of the $\tilde{B}$ and $\tilde{C}'$ states show long progressions in the ν_2' vibrational out-of-plane bending mode (umbrella motion), peaking in intensity around $\nu_2' = 7$. Although all of these vibronic states have been shown to be affected by predissociation,[4,18,26−29,33,34,41,45,49−51] most of them show sufficient rotational structure to allow for detailed investigations of the rotational levels and constants.[4,26−29,32,34−39,41,42,44,45,52] The investigations of the rotational structure have resulted in the determination of the excited-state symmetry, as well as in the correct numbering of the vibrational levels of the main progression based on ν_2'.[4,26,29,31−34,36,39,41,42]

Figure 3a shows the (2 + 1) REMPI excitation spectrum of NH_3 for the $\tilde{B}$ and $\tilde{C}'$ ν_2' vibrational members investigated in the present study using nanosecond excitation in combination with electron detection. The ν_2' numbering of the excited-state vibrational levels indicated at the top of Figure 3 has been adopted from the literature.[4,26,29,31−34,36,39,41,42] The excitation spectrum has not been corrected for the dye gain, but the individual connected parts have each been recorded at near-constant laser power. Three sections in Figure 3a have been lifted above the baseline to indicate that they are shown at an enlarged intensity scale (10×). It can be observed that the excitation spectrum is dominated by the $\tilde{C}'(\nu_2'=1,2)$ states. The $\tilde{B}(\nu_2'=6,7)$ states appear with considerably lower intensity, whereas in earlier (3 + 1) REMPI excitation spectra the $\tilde{B}$ and $\tilde{C}'$ resonances were of comparable intensity.[32,33,43] All states except the $\tilde{C}'(\nu_2'=3)$ state show distinct rotational structure.

Figure 3b shows the equivalent excitation spectrum of NH_3 obtained using picosecond excitation. A similar spectrum obtained with picosecond excitation for the ND_3 states examined in the present study is shown in Figure 4. This figure shows that in ND_3 several $\tilde{B}$ and $\tilde{C}'$ vibronic states overlap. The excitation spectra of Figures 3b and 4 have been recorded with the use of different dyes in the picosecond dye amplifier. Each individual part in these figures represents a different dye, and the picosecond excitation spectra have not been corrected for the dye gain. The rotational structure, which can be observed in the nanosecond excitation spectrum of NH_3 (Figure 3a), is to a large extent lost in the NH_3 picosecond excitation spectrum (Figure 3b) due to the large spectral width of the picosecond UV laser pulses. It is further apparent from Figure 3 that the $\tilde{B}$:$\tilde{C}'$ intensity ratio is considerably larger with picosecond excitation than with nanosecond excitation, indicating the delicate balance between ionization and decay processes in these states.

A discussion of the excitation spectra of the NH_3 $\tilde{C}'(\nu_2'=2)$ vibrational band obtained with nanosecond and picosecond excitation sources may serve in many respects as an example for the other states examined in the present study. The out-of-plane bending vibration ν_2' has a_2'' symmetry in the D_{3h} point group. It is by now well established that the $\tilde{C}'$ state has $^1A_1'$ electronic symmetry in D_{3h}.[31−33,41,42] The rovibronic symmetry of the $\tilde{C}'(\nu_2')$ vibrational members is therefore $^1A_1'$ for even ν_2' and $^1A_2''$ for odd ν_2'. Of the two-photon transition tensors only T^0_0 and T^2_0 with accompanying selection rules $\Delta J = 0$, $\Delta K = 0$, and $\Delta J = 0, \pm1, \pm2$, $\Delta K = 0$, respectively, possess the appropriate symmetry ($^1A_1'$) to induce transition intensity in the spectrum. The $\tilde{C}'(\nu_2')$ excited states with $^1A_1'$ ($^1A_2''$) rovibronic symmetry are thus connected with the $^1A_1'$ ($^1A_2''$) levels of the near-degenerate ground-state manifold. The T^0_0 tensor dominates the $\tilde{C}'$ spectra, providing nearly all intensity in the central Q-branch, while the T^2_0 tensor contributes only to a small extent, most notably in the wings of each absorption band.

The nuclear spin statistics of the ground state, which result from the fact that the three H atoms (I = 1/2) or D atoms (I = 1) in NH_3 or ND_3 are equivalent,[53,54] have a profound influence on the rotational contours. For the $\tilde{C}'(\nu_2'=2)$ band in NH_3 the

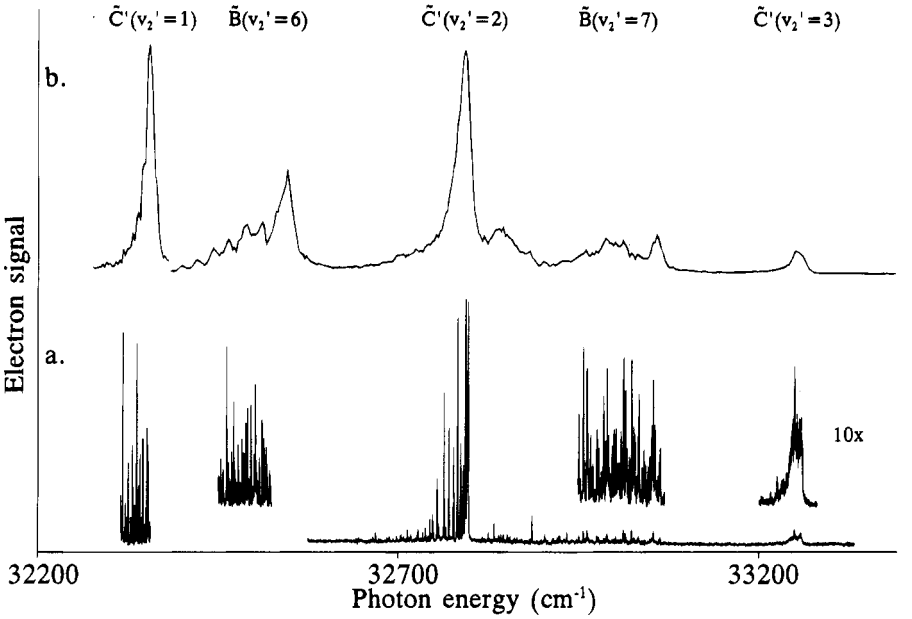

Figure 3. (2 + 1) REMPI excitation spectra of NH_3 obtained with nanosecond (a) and picosecond (b) excitation in combination with electron detection. The band assignments are given at the top of the figure.

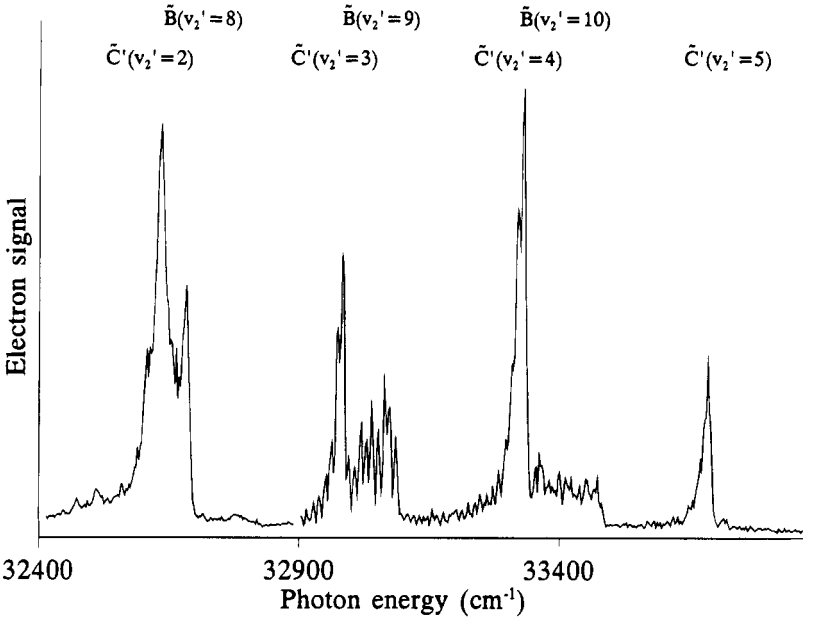

Figure 4. (2 + 1) REMPI excitation spectrum of ND_3 obtained with picosecond excitation in combination with electron detection. The band assignments are given at the top of the figure.

nuclear statistics are responsible for a relative enhancement of the transitions originating from rotational levels for which $K = 3n$, $n = 0, 1, 2...$(ortho levels) compared to transitions beginning in rotational levels with $K = 3n \pm 1$, $n = 0, 1, 2...$(para levels).

In the present study we have simulated the excitation spectrum of the $\tilde{C}'(v_2'=2)$ state and the excitation spectra of the other bands with a rotational contour program, which uses the known rotational constants of the ground state[1,2] and the excited state[26,29,45] to calculate the energies of the rotational levels associated with these states.[54] The intensities of the transitions between the rotational levels in the ground state and in the excited state are determined by a line-strength factor,[55] a Boltzmann factor including the rotational degeneracy as well as the temperature, and the nuclear spin statistics of the ground state. The rotational contour is calculated assuming a certain line shape for the transitions, which is dependent on whether nanosecond or picosecond excitation is employed (*vide infra*). Since the simulation using previously determined rotational constants of the $\tilde{C}'(v_2'=2)$ state in NH_3 exhibited systematic differences with the observed line positions, we have also performed a three-parameter fit on this band in order to obtain values for the B′ and C′ rotational constants as well as the rotationless transition energy T_0, which could describe the measured excitation spectrum more accurately. A six-parameter fit, in which the effects of the centrifugal parameters D_J, D_{JK}, and D_K were included, similar to previous studies on the $\tilde{C}'(v_2'=0,1)$ members,[45] yielded unreliable results in the present case. The resulting parameters are given in Table 1, together with previously reported values. Our results compare well with an earlier (2 + 1) study,[44] but significant differences occur between our (2 + 1) results and the most accurate (3 + 1) study.[26]

The NH_3 $\tilde{C}'(v_2'=2)$ excitation spectra obtained with nanosecond and picosecond excitation in combination with electron detection are shown on a larger energy scale in parts b and d of Figure 5, respectively. The resulting simulations using the

TABLE 1: Optimal Fit Parameters (cm^{-1}) for the $\tilde{C}'(v_2'=2)$ Vibrational Level in NH_3 Obtained from the Present Study and Reported in Previous Studies

	present study	ref 26	ref 32	ref 41	ref 44
T_0	65 601.9 ± 0.5		65 610		
B'	9.877 ± 0.005	9.91 ± 0.01	9.93 ± 0.05	9.93	9.88 ± 0.05
C'	5.392 ± 0.005	5.36 ± 0.01	5.35 ± 0.1	5.38	5.39 ± 0.05

rotational constants determined in our work are shown in Figure 5a for nanosecond and in Figure 5c for picosecond excitation. For the best nanosecond simulation a Lorentzian line shape with a width of 0.4 cm^{-1} (fwhm) was used, which indicates that the shape of the rotational lines is to a large extent determined by the natural line width. In the picosecond excitation spectrum, however, the best qualitative agreement with the experimental spectrum is obtained when a Gaussian line shape with a width of 12 cm^{-1} (fwhm) is used, indicating that the shape of the rotational contour is determined exclusively by the spectral width of the UV picosecond laser pulses. It can be seen that all rotational resolution is lost in the picosecond excitation spectrum, except for two partly resolved structures corresponding to the largest peaks in the nanosecond spectra. The strong rotational progression designated as $(J'',K'') \rightarrow\rightarrow (J' = J'',K' = K'')$, where the doubly primed rotational quantum numbers refer to the lower level and singly primed numbers to the upper level, has been marked at the top of Figure 5. This progression is the main contributor to the peaks with the largest intensity in the spectra.

When the heights of the rotational lines in the nanosecond experimental spectrum (Figure 5b) and the simulated spectrum (Figure 5a) are compared, it is clear that considerable differences occur. It is emphasized that these differences do not result from the dye gain or saturation effects. It is well-known that the final step in a (2 + 1) excitation and ionization scheme does not influence the individual rotational line intensities provided that two requirements are met. First, the final step must be wavelength independent, which would be expected in the present case. Secondly, rotational-level-dependent loss mechanisms, which might compete with the ionization step and depopulate the rotational levels associated with the excited state in a J',K'-dependent way, should not be of importance. From previous studies it is known that such loss mechanisms are operative in all Rydberg states of ammonia. Both radiative (fluorescence)[45,56,57] and nonradiative (predissociation)[4,18,26-29,33,34,41,49-51] processes have been observed. Figure 5a,b shows that the rotational transitions with high values of $J'' = K'' = J' = K'$ (≥ 6) have larger intensities in the experimental spectrum than in the simulated spectrum. This suggests that a loss mechanism is operative in the $\tilde{C}'(v_2'=2)$ vibrational state in NH_3, which is less effective for the rotational levels which are involved in the transitions whose intensity is too large in our experimental spectrum. In that case the competing ionization step produces more intensity in the electron or NH_3^+ ion excitation spectrum. From previous studies it is known that this loss mechanism should be ascribed to predissociation.[4,18,26-29,33,34,41,45,49-51]

The influence of predissociation has been observed before in the (3 + 1) excitation work on the $\tilde{C}'(v_2')$ states of NH_3 and ND_3.[26] In these studies it was shown that transitions to rotational levels of the $\tilde{C}'(v_2' \geq 4)$ vibrational members of ND_3 with high J',K' have an intensity which is smaller than would be expected from the simulations. The experimental spectrum could be reproduced reasonably well by invoking an additional attenuation factor $F = \{1 + c[J'(J' + 1) - (K')^2]\}$ to model a heterogeneous predissociation process. The above discussion implies that rotational levels in the excited state, for which associated transitions are weaker in the experimental spectrum

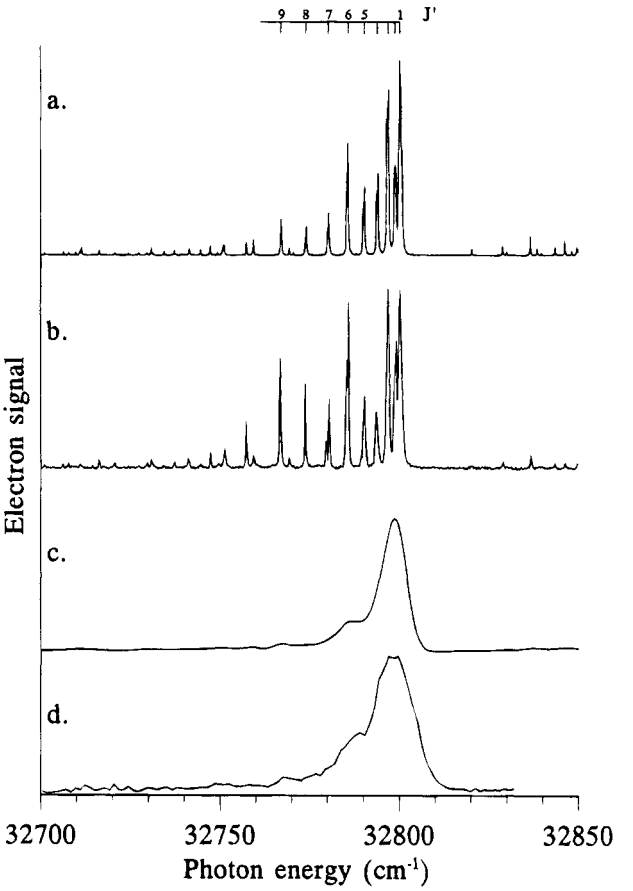

Figure 5. Experimental (2 + 1) REMPI excitation spectra of the $\tilde{C}'(v_2'=2)$ band in NH_3 obtained with nanosecond (b) and picosecond (d) excitation in combination with electron detection. The main progression, attributable to the $(J'',K'') \rightarrow\rightarrow (J',K' = J'',K'')$ transitions, is marked at the top of the figure. In the simulations of the nanosecond (a) and picosecond (c) excitation spectra a temperature of 293 K has been used. In part a Lorentzian line shapes with a width of 0.4 cm^{-1} (fwhm) have been assumed for the transitions, whereas in part c Gaussian line shapes with a width of 12 cm^{-1} (fwhm) have been employed.

than in the simulation, have a shorter lifetime than other rotational levels. The previous study thus shows that in ND_3 $\tilde{C}'(v_2' \geq 4)$ rotational levels for which J',K' are high have shorter lifetimes than the rotational levels for which J',K' are low. In contrast, the present results on the $\tilde{C}'(v_2'=2)$ vibrational level in NH_3 show the opposite behavior; that is, now the rotational levels with high J',K' are longer lived. We have observed a similar trend for the $\tilde{C}'(v_2'=1)$ state in NH_3. The heterogeneous predissociation is expected to be operational in the higher $\tilde{C}'(v_2')$ states of NH_3 as well, but a detailed investigation of this effect has been denied by lack of rotational resolution in the excitation spectra of these states due to a second, homogeneous, predissociation mechanism, which affects all rotational levels similarly. This homogeneous predissociation mechanism influences the $\tilde{C}'(v_2' \geq 3)$ states in NH_3, but has not been observed as yet for the $\tilde{C}'(v_2')$ states in ND_3 up to $v_2' = 7$.[26] A first effect of the homogeneous predissociation is the considerably reduced intensity in the REMPI excitation spectrum (see for example Figure 3a).

Figure 6a shows the nanosecond (2 + 1) REMPI excitation spectrum of the $\tilde{C}'(v_2'=3)$ vibrational state in NH_3 at an enlarged energy scale. It can be observed that most rotational lines are severely broadened, indicating short lifetimes (*vide infra*), but partly resolved rotational structure is still present, as has been reported previously for the (3 + 1) REMPI excitation spectrum of this state.[26,31,32] We have tried to simulate this spectrum using

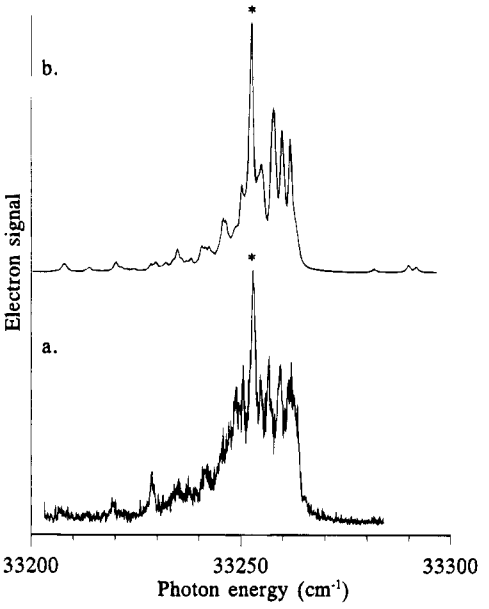

Figure 6. Experimental (2 + 1) REMPI excitation spectrum of the $\tilde{C}'(v_2'=3)$ band in NH_3 obtained with nanosecond excitation in combination with electron detection (a). Part b shows the corresponding simulation. In the simulation a temperature of 293 K and Lorentzian line shapes with a line width of 2.0 cm^{-1} (fwhm) for the transitions have been used. The intensity of the peak marked with an asterisk, presumably corresponding to the (6,0) → → (6,0) transition, has been multiplied by an additional factor of 7.5.

the rotational constants from the literature[32] ($B' = 9.49\ cm^{-1}$, $C' = 5.60\ cm^{-1}$). However, the peak positions could not be reproduced in this way, leading to an overall blended rotational contour, which did not resemble our experimental result. On the other hand, a detailed rotational analysis with our experimental results is not possible. We have therefore changed the rotational constants in the simulation slightly from the values in the literature, until a good agreement was obtained with the experimental spectrum ($B' = 9.39\ cm^{-1}$, $C' = 5.57\ cm^{-1}$). It then became immediately clear that there is at least one transition, marked in Figure 6a, whose intensity is considerably underestimated in the simulation. It would seem that the rotational level in the excited state associated with this transition has a substantially longer lifetime than the other levels, as discussed above. Unambiguous identification of this level is hampered by the lack of precise values for the rotational constants in the excited state, but it would seem that it is the $(J'',K'' = 6,0) \rightarrow\rightarrow (J',K' = 6,0)$ transition which dominates the experimental excitation spectrum. Figure 6b shows a simulation in which the intensity of this transition has been increased by an additional factor of 7.5. The agreement between the experimental and simulated spectra is now reasonably good.

The $\tilde{B}$ state is electronically degenerate with symmetry $^1E''$ in D_{3h}.[4,28,29,34,39,54] Just as in the case of the $\tilde{C}'(v_2')$ states, the v_2' vibrational levels in the $\tilde{B}$ state have alternating vibronic symmetry: $^1E''$ for even v_2' and $^1E'$ for odd v_2'. The two-photon transition tensors $T^2_{\pm 1}$, which transform as $^1E''$ in D_{3h}, carry the transition intensity for the $^1A_1' \rightarrow\rightarrow\ ^1E''$ and $^1A_2'' \rightarrow\rightarrow\ ^1E'$ transitions, resulting in the two-photon selection rules $\Delta J = 0, \pm 1, \pm 2$ and $\Delta K = \pm 1$ for the $\tilde{B}$ state. The $T^2_{\pm 2}$ two-photon transition tensors, which transform as $^1E'$ in D_{3h}, with accompanying selection rules $\Delta J = 0, \pm 1, \pm 2$ and $\Delta K = \pm 2$, would also possess the correct symmetry to contribute to the $\tilde{B}$ two-photon excitation strength, but it has been confirmed experimentally that its contributions are negligible.[37,39] Earlier studies have led to an accurate description of the spectroscopic properties of the $\tilde{B}(v_2')$ vibrational levels.[4,29,34,39] The two degenerate components of the $^1E''$ electronic state are described by the vibronic quantum number l, which can take the values ± 1. The $|J',K',M'\rangle|l = -1\rangle$ wave functions are coupled to the $|J',K' + 2,M'\rangle|l = +1\rangle$ wave functions, resulting in additional shifts in the rotational level positions and a splitting between the rotational levels with $^1A_1'$ ($^1A_1''$) and $^1A_2'$ ($^1A_2''$) symmetry for the $K' = 1$ levels associated with the vibrational members with $^1E''$ ($^1E'$) vibronic symmetry. Furthermore, the intensities of transitions to the rotational levels in the $\tilde{B}(v_2')$ states are influenced by this coupling effect, which is particularly important for rotational levels with high values of J'. The coupling effect is described by an additional parameter q and is responsible for the l-type doubling in the $\tilde{B}$ state.

All excitation spectra of the $\tilde{B}(v_2')$ vibrational levels studied in the literature show well-resolved rotational structure. Due to the perpendicular nature of the transitions to the $\tilde{B}(v_2')$ states, they appear in the excitation spectra with large numbers of rotational lines confined to a small energy region. This can be seen, for example, in the excitation spectra of the $\tilde{B}(v_2'=6,7)$ states examined in the present study (see Figure 3a). We have simulated these spectra for NH_3 using our rotational contour program and the excited-state parameters as determined previously.[29,39] The nanosecond excitation spectra are best described by assuming a Lorentzian-shaped line form with a width of about 0.9 cm^{-1} (fwhm) for the rotational lines. This large line width is the first indication that the lifetimes of the $\tilde{B}$ state rotational levels are shorter than for the $\tilde{C}'(v_2'=1,2)$ states. There is qualitative agreement with the fact that the $\tilde{B}(v_2'=6,7)$ states in NH_3 have less intensity than the $\tilde{C}'(v_2'=1,2)$ states in the excitation spectra. The picosecond excitation spectra of the $\tilde{B}(v_2'=6,7)$ vibrational members in NH_3 (Figure 3b) can now be simulated quite well by changing the line shape to Gaussian with a width (fwhm) of 12 cm^{-1}. The heights of the individual rotational lines in the experimental $\tilde{B}(v_2'=6,7)$ spectra can be reproduced satisfactorily in the simulations, and rotational-level-dependent deviations as described above for the $\tilde{C}'$ states are not observed. This suggests that all rotational levels associated with one of the $\tilde{B}(v_2'=6$ or 7) vibrational levels have similar lifetimes; that is, the $\tilde{B}(v_2')$ states show considerably less evidence of rotational-level-dependent predissociation than the $\tilde{C}'(v_2')$ states.

III.B. Natural Line Width Measurements. In the previous section we have been concerned with the excitation spectra of several vibrational members of the $\tilde{B}$ and $\tilde{C}'$ states of NH_3 and ND_3. In particular, it has been observed that as the result of predissociation, the intensities of rotational transitions might be reduced. The influence of such predissociation mechanisms will also be apparent in the natural lifetimes of rotational levels associated with the excited states. These lifetimes within different v_2' vibrational levels in the $\tilde{B}$ and $\tilde{C}'$ states of NH_3 and ND_3 have been determined in previous studies using accurate line width measurements.[27,29] The natural lifetime τ of an excited state is correlated to the natural line width Γ of transitions to this level in the excitation spectrum by $\Gamma\tau = (2\pi c)^{-1}$. In order to extract the natural line width, and hence the natural lifetime, from the excitation spectrum, several conditions must be satisfied to avoid spectral broadening caused by sources other than the natural lifetime. First and most important, the spectral width of the excitation light must be smaller than the natural line width. Secondly, mechanisms such as pressure, collisional, Doppler, and laser power broadening must be preferably excluded or corrected for. Thirdly, to determine the exact line width, a specific line shape has to be assumed for the spectral line, which introduces uncertainties in the lifetime. Furthermore, it is not always possible to observe

an individual line as the result of blending of several rotational lines. The above conditions are not always easily satisfied, and it is often extremely difficult to measure the exact lifetimes reliably *via* the natural line widths. A lower limit for the lifetime, on the other hand, can in most cases be obtained without difficulty.

A typical natural lifetime in the present study on ammonia is 100 ps, corresponding to a natural line width of 0.05 cm^{-1}. To measure line widths of this magnitude, a specialized experimental setup is required. In previous studies of Ashfold *et al.* sub-Doppler spectroscopy has been applied using a high-power excitation source with a bandwidth of 0.008 cm^{-1} at the excitation energies required for the $\tilde{B}$ and $\tilde{C}'$ states in ammonia.[27,29] These studies have shown that heterogeneous predissociation plays a major role in the $\tilde{C}'(v_2'=2)$ vibrational level of ND_3.[27] The natural line width of the $(J'',K'' = 0,0) \rightarrow \rightarrow (J',K' = 0,0)$ transition was measured as 0.012 cm^{-1}, corresponding to a lifetime of the $(J',K' = 0,0)$ level of 450 ± 100 ps. The uncertainty in the lifetime resulted from the corrections that needed to be applied for some of the broadening mechanisms described above, as well as from the assumptions concerning the line shape. In a study on the line widths of transitions to rotational levels associated with the $\tilde{B}(v_2')$ vibrational states lifetimes of 250 ± 20 ps for ND_3 and 6.1 ± 0.7 ps for NH_3 were found. These values were reported to be independent of v_2', J', and K' in all studied vibrational levels ($v_2' \leq 6$ for ND_3 and $v_2' \leq 8$ for NH_3).[29]

The two-UV-photon laser bandwidth of our nanosecond excitation source is about 0.3 cm^{-1} and consequently only allows for the natural line width measurement of transitions to rotational levels with a lifetime shorter than about 15 ps. We have confirmed for the $\tilde{B}(v_2'=6,7)$ levels in NH_3 that the line shapes of the rotational transitions are well described by Lorentzian forms with natural widths (fwhm) of about 0.65−0.90 cm^{-1}, corresponding to natural lifetimes of 6−8 ps, in agreement with the earlier study. Our nanosecond excitation source does not allow for a detailed line width investigation of the $\tilde{C}'(v_2')$ states in NH_3 and ND_3 or the $\tilde{B}(v_2')$ states in ND_3, because the transitions to rotational levels in these states have natural line widths on the order of or significantly smaller than the bandwidth of our excitation source.

III.C. Photoelectron Spectra. The REMPI photoelectron spectra (PES) for NH_3 have previously been measured using (2 + 1) and (3 + 1) ionization schemes *via* several $\tilde{B}(v_2')$ and $\tilde{C}'(v_2')$ vibrational levels.[36,43,58,59] Both the $\tilde{B}$ and $\tilde{C}'$ excited states as well as the $\tilde{X}\ ^2A_2''$ ionic ground state have planar geometries, and the REMPI photoelectron spectra are consequently expected to be dominated by $\Delta v = 0$ photoelectron peaks; that is, the ion is produced with the same vibrational quantum numbers as the excited state from which ionization took place. This has been confirmed experimentally insofar as the total energy of the photons suffices to produce the expected state-selected ions.[36,43,58,59] As the ν_2 vibration is most important upon excitation from the ground state, the photoelectron spectra *via* the different v_2' vibrational members of the $\tilde{B}$ and $\tilde{C}'$ states consist almost exclusively of intense $\Delta v_2 = 0$ transitions. In a previous (2 + 1) REMPI−PES study it has been shown that small photoelectron peaks corresponding to $\Delta v_2 = \pm 1$ transitions are present as well.[36] In photoelectron spectra obtained by (2 + 1) ionization *via* the $\tilde{B}(v_2'=3-5,7-10)$ states a number of photoelectron peaks on the low energy side of the $\Delta v_2 = 0,\pm 1$ peaks were found to be responsible for a contamination of about 10% to the state-selected ionization process. The strongest of these peaks, which are not observed for (2 + 1) ionization *via* the $\tilde{C}'(v_2')$ states, was found in a subsequent (2 + 1) study on the $\tilde{B}(v_2'=10)$ in NH_3 to be located at an energy difference of 0.40 ± 0.02 eV from the main $\Delta v_2 = 0$ peak. For this photoelectron peak an assignment as $\tilde{X}\ ^2A_2''(10\nu_2^+ + \nu_3^+)$ was suggested.[59]

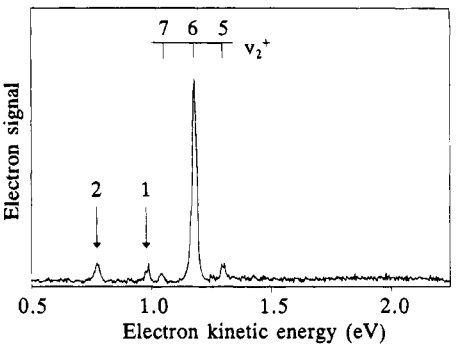

Figure 7. Photoelectron spectrum obtained for (2 + 1) ionization *via* the $\tilde{B}(v_2'=6)$ state in NH_3 ($h\nu$ = 32 499 cm^{-1}). The assignments are given at the top of the figure. The peaks labeled 1 and 2 are discussed in the text.

TABLE 2: Vibrational Frequencies (eV) in the Ground State of Neutral Ammonia and the Ammonia Cation As Determined in the Present and in Previous Studies

	NH_3[a]	ND_3[a]	NH_3^+	ND_3^+
$\nu_1(a_1')$	0.414	0.300	0.391 ± 0.012[c]	
			0.404 ± 0.007[e]	0.304 ± 0.007[e]
$\nu_2(a_2'')$	0.116[b]	0.093	0.111[d]	0.090[d]
	0.120[b]			
$\nu_3(e')$	0.423	0.317	0.420[d]	
$\nu_4(e')$	0.202	0.148	0.197 ± 0.007[e]	0.141 ± 0.007[e]

[a] Reference 53. [b] Inversion doubling components. [c] Reference 60. [d] Reference 68. [e] Present study.

In the present study we have measured the (2 + 1) REMPI−PES spectra *via* the $\tilde{B}(v_2'=2-12)$ and $\tilde{C}'(v_2'=0-8)$ vibrational members in NH_3 using the nanosecond excitation source. The photoelectron spectra are, as far as the strongest photoelectron peaks are concerned, similar to the spectra obtained in previous (2 + 1) studies.[36,59] A typical photoelectron spectrum obtained by excitation *via* the $\tilde{B}(v_2'=6)$ state is shown in Figure 7. The spectrum shows the $\Delta v_2 = 0,\pm 1$ peaks as well as the photoelectron peaks on the low energy side of the spectrum, labeled 1 and 2 in Figure 7. In all $\tilde{B}(v_2')$ photoelectron spectra measured in the present study the latter peaks are located at 0.197 ± 0.007 eV for peak 1 and 0.404 ± 0.007 eV for peak 2 below the $\Delta v_2 = 0$ peak. It therefore seems likely that these peaks should be assigned to a progression in the $\tilde{X}\ ^2A_2''$ ground ionic state, which consists of the main $n\nu_2^+$ progression plus an extra amount of vibrational excitation, as suggested earlier.[59] The known vibrational frequencies of the ground states of neutral ammonia and the ammonia cation are listed in Table 2. The frequencies in the ground state of the cation, determined from the present results, are also given in Table 2. The assignment of peak 1 is in the first instance problematic, since none of the known vibrational frequencies of the ground state of the NH_3^+ ion match the measured interval of 0.197 eV. Inspection of the vibrational frequencies in the ground state of the neutral shows that the asymmetric bending vibration has a frequency of 0.202 eV in this state. In view of the similarity of these two frequencies we therefore assign peak 1 to $\tilde{X}\ ^2A_2''(n\nu_2^+ + \nu_4^+)$. Evidence of activity of the ν_4^+ vibration in the ground state of NH_3^+ has also been observed recently in a high-resolution ZEKE study.[40] Due to the near-equivalence of different vibrational excitations in the ion, several assignments are possible for peak 2. The ν_3^+ vibrational frequency in the ionic ground state is just outside the experimental uncertainty in our results to assign

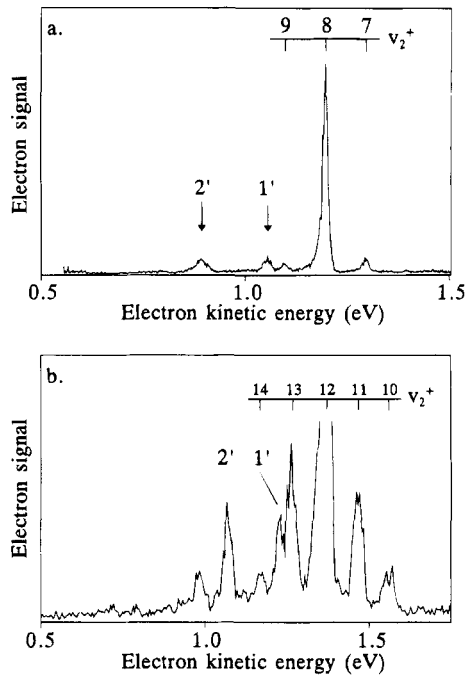

Figure 8. Photoelectron spectra obtained for (2 + 1) ionization *via* the $\tilde{B}(v_2'=8)$ state ($h\nu$ = 32 635 cm^{-1}, a) and the $\tilde{B}(v_2'=12)$ state ($h\nu$ = 34 146 cm^{-1}, b) in ND_3. Assignments are given at the top of the figures. The peaks labeled 1′ and 2′ are discussed in the text.

this peak to $\tilde{X}\ ^2A_2''(nv_2^+ + v_3^+)$. Several $\tilde{C}'\ 1^12^n$ bands in the excitation spectra of NH_3 and ND_3 have been observed by Miller *et al.* in a (2 + 1) REMPI–PES study.[60] From the photoelectron spectra, obtained for ionization *via* these bands, the ν_1^+ vibrational frequency in the ground state of NH_3^+ was determined as 0.391 ± 0.012 eV. In the present study we have remeasured the ν_1^+ frequency from the photoelectron spectra obtained at the $\tilde{C}'\ 1^12^1$, 1^12^2 bands and obtained a value of 0.401 ± 0.007 eV, in agreement with the value of Miller *et al.* Peak 2 in the photoelectron spectra obtained for excitation *via* the $\tilde{B}(v_2')$ states can then be assigned to $\tilde{X}\ ^2A_2''(nv_2^+ + v_1^+)$. It is, however, also possible to assign this peak to $\tilde{X}\ ^2A_2''(nv_2^+ + 2v_4^+)$, because the energy difference between peak 2 and the $\Delta v_2 = 0$ peak is exactly twice the energy difference between peak 1 and the $\Delta v_2 = 0$ peak. In view of the assignments of the ND_3 photoelectron spectra (*vide infra*) we favor the former $\tilde{X}\ ^2A_2''(nv_2^+ + v_1^+)$ assignment.

To our knowledge there have been no previous reports of photoelectron spectra obtained *via* $\tilde{B}(v_2')$ or $\tilde{C}'(v_2')$ vibrational levels of ND_3. In the present study we have measured the (2 + 1) REMPI photoelectron spectra of the $\tilde{C}'(v_2'=0-7)$ vibrational members in ND_3. As in the case of NH_3, the $\Delta v_2 = 0$ ionization process dominates these spectra, and deviations in the form of $\Delta v_2 = \pm 1$ photoelectron peaks are small. We have also examined the photoelectron spectra obtained for ionization *via* several $\tilde{B}(v_2')$ states in ND_3 to investigate the behavior of the peaks which are equivalent to the peaks labeled 1 and 2 in the NH_3 photoelectron spectra. These photoelectron spectra are very similar to the NH_3 spectra, as can be seen from Figure 8a, which shows the photoelectron spectrum obtained for ionization *via* the $\tilde{B}(v_2'=8)$ vibrational level. The peaks labeled 1′ and 2′, located at photoelectron energies of 0.141 ± 0.007 and 0.304 ± 0.007 eV below the main $\Delta v_2 = 0$ photoelectron peak, are equivalent to the peaks labeled 1 and 2 in the NH_3 spectra. For higher members of the $\tilde{B}(v_2')$ progression the photoelectron spectra show an increasing v_2^+ activity other than $\Delta v_2 = 0$. Figure 8b shows the photoelectron spectrum obtained for excitation *via* $\tilde{B}(v_2'=12)$. The dominant $\Delta v_2 = 0$ photoelectron peak is cut off in Figure 8b in order to emphasize the weaker photoelectron peaks. The positions of the photoelectron peaks in Figure 8b are given in the Table 3, along with their assignments. Apart from the $\Delta v_2 = 0, \pm 1$ photoelectron peaks, $\Delta v_2 = \pm 2$ transitions are now also observed, as well as the peaks labeled 1′ and 2′. In the spectrum an extra peak is present, which was not observed in the previously discussed photoelectron spectra. This peak, with a photoelectron energy of 0.980 eV, is located 0.390 eV from the $\Delta v_2 = 0$ peak and can therefore be assigned to $\tilde{X}\ ^2A_2''(13v_2^+ + v_1^+)$, *i.e.*, the $\Delta v_2 = +1$ peak with an additional ν_1^+ quantum. The photoelectron peak corresponding to ions in the $\tilde{X}\ ^2A_2''(13v_2^+ + v_4^+)$ state is not observed. In contrast to NH_3, the energy difference between peak 2′ in ND_3 and the main $\Delta v_2 = 0$ peak is no longer exactly twice the energy difference between peak 1′ and the $\Delta v_2 = 0$ peak. On the basis of the above observations we favor the assignment of $\tilde{X}\ ^2A_2''(nv_2^+ + v_1^+)$ for peak 2′ (peak 2 in NH_3) over the $\tilde{X}\ ^2A_2''(nv_2^+ + 2v_4^+)$ assignment. The values reported in the present study for the ν_1^+ and ν_4^+ vibrations in the ground state of ND_3^+ are listed in Table 2 and are to our knowledge the first determinations of these frequencies in ND_3^+.

TABLE 3: Observed Kinetic Energies and Assignments of Photoelectron Peaks in the Photoelectron Spectrum Obtained for Ionization *via* the $\tilde{B}(v_2'=12)$ Vibrational Level of ND_3, Employing an Excitation Wavelength of 34 146 cm^{-1}

observed electron kinetic energy (eV)	ionic state
0.980	$\tilde{X}\ ^2A_2''(13v_2^+ + v_1^+)$
1.071	$\tilde{X}\ ^2A_2''(12v_2^+ + v_1^+)$
1.172	$\tilde{X}\ ^2A_2''(14v_2^+)$ and/or $\tilde{X}\ ^2A_2''(11v_2^+ + v_1^+)$
1.232	$\tilde{X}\ ^2A_2''(12v_2^+ + v_4^+)$
1.264	$\tilde{X}\ ^2A_2''(13v_2^+)$
1.370	$\tilde{X}\ ^2A_2''(12v_2^+)$
1.466	$\tilde{X}\ ^2A_2''(11v_2^+)$
1.563	$\tilde{X}\ ^2A_2''(10v_2^+)$

As a result of the pyramidal to planar geometry change, the He I photoelectron spectrum of the $\tilde{X}\ ^2A_2''$ ionic ground state shows the same ν_2 activity which is also observed in the excitation spectra of the $\tilde{B}(v_2')$ and $\tilde{C}'(v_2')$ Rydberg states. The v_2^+ progression peaks at approximately $v_2^+ = 7$, and the $v_2^+ = 0$ photoelectron peak at the position of the adiabatic ionization energy has a very low intensity.[61,62] The exact numbering of this progression in the ion, and hence the value of the adiabatic ionization energy, has been the subject of recent discussion. In an earlier study the adiabatic ionization energy was placed at 10.183 eV, and an additional photoelectron peak at a lower energy of 10.073 eV was interpreted as the 2_1^0 hot band.[62] These assignments have been questioned in a recent study,[63] in which the adiabatic ionization energy was set at 10.073 eV, thus changing the v_2^+ numbering of all peaks in the main progression by one quantum. In the present study we have been able to identify the photoelectron peak at 10.183 eV as the adiabatic ionization energy on the basis of the (2 + 1) REMPI–PES results *via* the $\tilde{B}(v_2')$ and $\tilde{C}'(v_2')$ states and the assumptions that the v_2' vibrational numbering in these excited Rydberg states is correct and that ionization of these states indeed occurs with a $\Delta v = 0$ propensity. This v_2^+ numbering is also in agreement with the results from a recent ZEKE study on NH_3.[40]

In the photoelectron spectra obtained with (2 + 1) REMPI *via* the $\tilde{B}$ or $\tilde{C}'$ states we have not observed differences between the spectra obtained with nanosecond and picosecond excitation, in agreement with a previous study in which picosecond excitation was used.[59] The photoelectron peaks deriving from ionization *via* $\tilde{B}(nv_2')$ and $\tilde{C}'(mv_2')$ states, at excitation energies where different vibrational levels of these two states overlap,

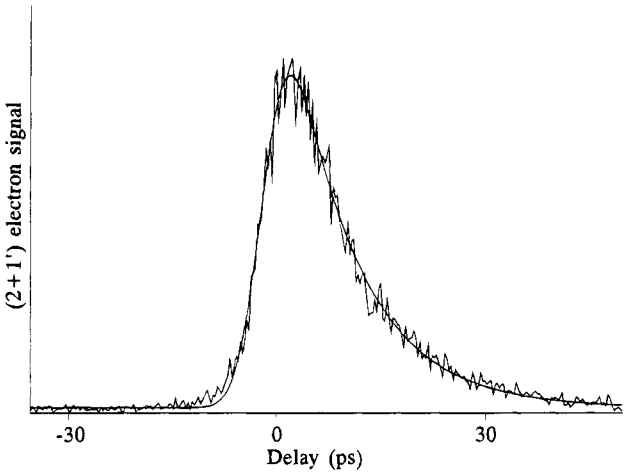

Figure 9. Experimental (2 + 1′) decay trace obtained for ionization *via* the $\tilde{B}(v_2'=6)$ vibrational level in NH_3 ($h\nu$ = 32 510 cm^{-1}). The solid line represents the best fit, which assumes a monoexponential decay with a time constant of 9.3 ps.

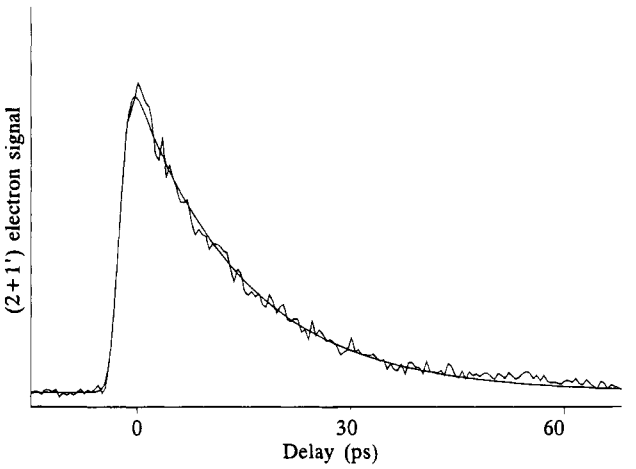

Figure 10. Experimental (2 + 1′) decay trace obtained for ionization *via* the $\tilde{C}'(v_2'=3)$ vibrational level in NH_3 ($h\nu$ = 33 200 cm^{-1}). The solid line represents the best fit, which assumes a monoexponential decay with a time constant of 15 ps.

are always separated by an amount which enables unambiguous identification of the state under investigation. This energy difference $(n - m)v_2^+$ is about $5v_2^+$ for NH_3 and $6v_2^+$ for ND_3. The simple appearance of the photoelectron spectra allows for an immediate identification of the (2 + 1) and (2 + 1′) electron signals in the two-color experiments using picosecond excitation, even in cases where different $\tilde{B}(v_2')$ and $\tilde{C}'(v_2')$ vibrational members overlap.

III.D. Picosecond Real-Time Lifetime Measurements. In a previous section it has been described how the natural lifetimes of rotational levels associated with the vibrational components of the $\tilde{B}$ and $\tilde{C}'$ Rydberg states could be determined indirectly from accurate natural line width measurements. In the present study the lifetimes have been measured in real time in a pump–probe setup, which has been described above. The pump pulse excites the rotational levels associated with the $\tilde{B}(v_2')$ or $\tilde{C}'(v_2')$ Rydberg state under investigation, while the probe pulse subsequently ionizes the molecule in a one-photon absorption step with a strong $\Delta v = 0$ propensity. The decrease in the (2 + 1′) two-color photoelectron signal is monitored as a function of the delay time between the pump and probe pulses and reflects the depopulation of the excited state. In the present study we have examined in real time the lifetimes of the rotational levels in the $\tilde{B}(v_2')$ and $\tilde{C}'(v_2')$ vibrational members, for which the excitation spectra are shown in Figures 3 and 4.

A typical decay trace is shown in Figure 9, where the (2 + 1′) decay obtained for ionization *via* the NH_3 $\tilde{B}(v_2'=6)$ vibrational level is depicted. Due to the large excitation bandwidth of the picosecond laser system, it is expected that several rotational levels within the $\tilde{B}(v_2'=6)$ vibrational level are coherently excited, as shown above in the discussion of the picosecond excitation spectra. The decay trace in Figure 9 is determined by the convolution of the system response and the exponential decay, and its analysis may serve as an example for the other decay traces measured in the present work. The (2 + 1′) electron signal first rises to a maximum value around delay time zero, with a temporal behavior determined by the system response. In Figure 9 as well as in all other real-time decay traces measured in the present study the probe pulse was generated by frequency mixing the output of the picosecond dye amplifier and the regenerative amplifier. Such a pulse was found to have a pulse width of about 4 ps (fwhm). The temporal width of the system response is consequently about 5 ps, as can be observed in Figure 9. For positive delay times the (2 + 1′) electron signal decreases to zero, with a temporal behavior determined by both the system response and the natural lifetime of the excited state. In order to extract the lifetime of the excited state from Figure 9, a deconvolution procedure is required. The traces are assumed to be described by a convolution of a Gaussian-shaped system response function and a mono- or biexponential decay and are fitted using a nonlinear least-squares algorithm. The traces are thus described by the following parameters: the position of delay time zero t_0, the width (fwhm) of the Gaussian system response, the preexponential factor(s), and the decay time(s) $\tau_1(\tau_2)$. The best fit for the $\tilde{B}(v_2'=6)$ state, using a monoexponential decay with a time constant of 9.3 ps, is shown in Figure 9 as the smooth solid curve and describes the measured decay quite adequately. The experimental traces are found to be less accurately described when other line shapes, such as Lorentzian or $sech^2$, are assumed for the system response. It was typically found that the width of the Gaussian-shaped system response varied somewhat from day to day (±10%), but it was always nearly constant within one measurement session.

Figure 10 shows the decay trace of the NH_3 $\tilde{C}'(v_2'=3)$ vibrational state together with the best fit. In this case the femtosecond dye laser has been used to produce the pump pulse, and its output was frequency-mixed with the output of the regenerative amplifier to give the probe pulse. The time resolution of 2.5 ps is considerably better than in Figure 9, and the use of a monoexponential decay results in a decay time of 15 ps.

Figure 11 shows a series of five decay traces (labeled 1–5) obtained at different wavelengths in the excitation spectrum of the ND_3 $\tilde{C}'(v_2'=3)$ vibrational level. The one-photon energy difference between two adjacent traces is about 6 cm^{-1}. Trace number 1 has been recorded at the excitation wavelength which gives the maximum signal. From the simulations of the excitation spectra described above we know that this wavelength corresponds to transitions to rotational levels with low values for J',K' in the excited state. It can be observed that these levels have comparatively long lifetimes, and, as a consequence, the ionization signal has not decreased to zero at the maximum delay imposed by the finite length of the translational stage. This fact introduces uncertainties in the exponential decay parameter(s) that result from the fitting procedure. The lifetime uncertainty in decay traces where the natural lifetime is on the same order as the width of the system response is to a major extent determined by assumptions about the shape of the system response. For long decays of the kind shown in Figure 11

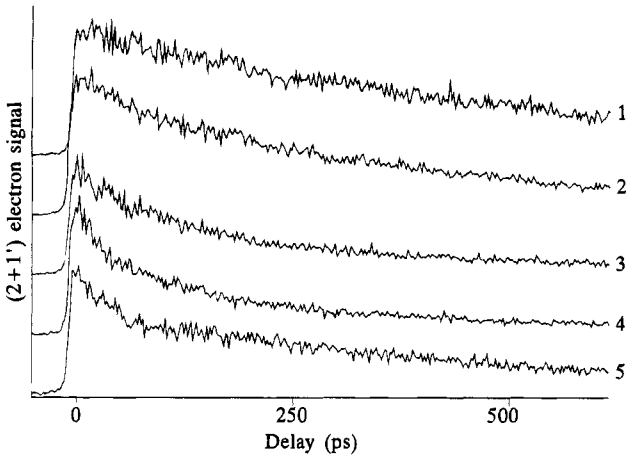

Figure 11. ND_3 (2 + 1′) decay traces obtained at different positions in the excitation spectrum of the $\tilde{C}'(v_2'=3)$ state. The decays labeled 1 and 2 are monoexponential with decay times of 535 and 385 ps, respectively. The traces labeled 3, 4, and 5 are biexponential with decay times of $\tau_1 = 100$ ps and $\tau_2 = 500$ ps for 3, $\tau_1 = 46$ ps and $\tau_2 = 360$ ps for 4, $\tau_1 = 26$ ps and $\tau_2 = 500$ ps for 5. The decay labeled 1 has been obtained using an excitation wavelength of 32 980 cm^{-1}. In each subsequent trace the one-photon energy has been decreased by 6 cm^{-1}.

assumptions about the system response are of no importance. When the pump wavelength is tuned toward the region in the excitation spectrum where transitions to higher J',K' rotational levels are located, it can be seen from Figure 11 that the temporal behavior can no longer be described accurately by a monoexponential decay. The traces labeled 2−5 in Figure 11 turn out to require a description by a biexponential decay. This is particularly clear in the traces numbered 4 and 5 in Figure 11.

Biexponential decay has been observed for the $\tilde{C}'(v_2'=3,4,5)$ vibrational levels in ND_3. This effect can be understood qualitatively if it is assumed that several transitions to different J',K' rotational levels are coherently excited by the picosecond laser pulse and contribute to the ionization signal. In principle, one would expect that if several transitions to rotational levels in the excited state with different lifetimes are coherently excited, the decay traces would be described by a multiexponential decay. However, for the traces measured in the present study one or two time constants were sufficient to describe the temporal decay behavior. These observations suggest that rotational levels with high J',K' values lying at lower energies in the excitation spectra of the $\tilde{C}'(v_2'=3,4,5)$ vibrational members in ND_3 have shorter lifetimes than the rotational levels with low J',K' values.

In the way described above we have measured in real time the natural lifetimes of the rotational levels associated with several vibrational states of the $\tilde{B}$ and $\tilde{C}'$ states in NH_3 and ND_3. The results are listed in Table 4. The rotational levels are in some cases described as J',K' = low and J',K' = high for reasons mentioned above in the discussion of Figure 11. If the decay behavior is monoexponential, only one lifetime is listed; in case of a biexponential decay the second time constant is given as well.

If the fourth harmonic of Nd:YLF from the regenerative amplifier is used as the probe pulse, (2 + 1′) excitation spectra at different fixed delay times between the pump and probe pulses can be obtained. Even though the time resolution is in this case only about 30 ps, these excitation spectra can provide valuable information, as will become clear from the following. Figure 12a shows two (2 + 1′) picosecond excitation spectra of the ND_3 $\tilde{C}'(v_2'=4)$ vibrational band obtained at fixed delay times

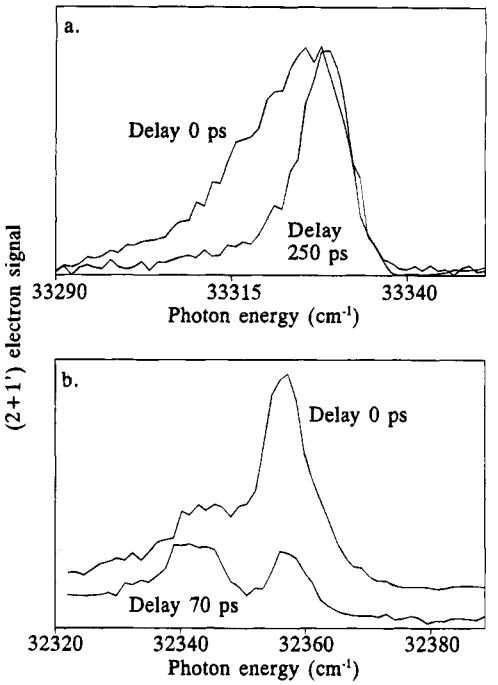

Figure 12. Picosecond excitation spectra of the $\tilde{C}'(v_2'=4)$ vibrational band in ND_3 (a) and the $\tilde{C}'(v_2'=1)$ state in NH_3 (b), in which the electrons deriving from the two-color (2 + 1′) ionization process are monitored. The fixed time delay between the pump pulse and the probe pulse is given.

TABLE 4: Decay Times and Decay Characteristics Obtained from the Real-Time Picosecond Experiments

vibronic state		decay time(s) (ps)	excitation wavelength (cm^{-1})
		NH_3	
$\tilde{B}(v_2'=6)$		$\tau = (6.8-9.4) \pm 0.4$	32 510−32 560
$\tilde{B}(v_2'=7)$		$\tau = 8.2 \pm 0.4$	33 060
$\tilde{C}'(v_2'=1)$	J',K' = low	$\tau = 25 \pm 5$	32 358
	J',K' = high	$\tau = 100 \pm 5$	32 340
$\tilde{C}'(v_2'=2)$	J',K' = low	$\tau = 15 \pm 2$	32 800
	J',K' = high	$\tau = 25 \pm 2$	32 787
$\tilde{C}'(v_2'=3)$		$\tau = 15 \pm 2$	33 200
		ND_3	
$\tilde{B}(v_2'=8)$		$\tau = (75-89) \pm 10$	32 685
$\tilde{B}(v_2'=10)$		$\tau = 70 \pm 10$	33 450
$\tilde{C}'(v_2'=2)$	J',K' = low	$\tau = 380 \pm 80$	32 640
	J',K' = high	$\tau = 410 \pm 80$	32 625
$\tilde{C}'(v_2'=3)$	J',K' = low	$\tau = 380 \pm 80$	32 980
	J',K' = high	$\tau = 45 \pm 5$	32 965
		$\tau_2 = 350 \pm 80$	
$\tilde{C}'(v_2'=4)$	J',K' = low	$\tau = 530 \pm 100$	33 330
	J',K' = high	$\tau_1 = 27 \pm 5$	33 320
		$\tau_2 = 280 \pm 50$	
$\tilde{C}'(v_2'=5)$	J',K' = low	$\tau = 130 \pm 20$	33 685
	J',K' = high	$\tau_1 = 23 \pm 5$	33 670
		$\tau_2 = 140 \pm 20$	

of 0 and 250 ps, as marked in the figure. The excitation spectrum at delay time 0 ps corresponds to the regular one-color excitation spectrum shown before in Figure 4. In Figure 12a only the photoelectrons originating from ionization of $\tilde{C}'(v_2'=4)$ have been monitored, whereas in Figure 4 the total electron signal, which includes electrons deriving from ionization of the overlapping $\tilde{B}(v_2'=10)$ level, was shown. The most striking difference between the excitation spectrum obtained at a delay time of 0 ps and the spectrum obtained at a fixed delay of 250 ps is the difference in width. In the latter excitation spectrum the transitions to the rotational levels with high values for J',K' have a considerably reduced intensity with respect to the intensity of the transitions to the rotational levels with low

values for J',K'. This shows unambiguously that the rotational levels with high J',K' have shorter lifetimes than the rotational levels with low J',K'. The same behavior is observed for the ND_3 $\tilde{C}'(v_2'=3,5)$ levels and is in qualitative agreement with the above observation of a biexponential decay for excitation on the low energy side of the maximum. Similar (2 + 1′) excitation spectra of the ND_3 $\tilde{C}'(v_2'=2)$ vibrational member at different fixed delay times between the pump and probe pulses show no dependence on the delay time, again in agreement with the real-time lifetime results from Table 4, which do not show biexponential decay profiles at any excitation wavelength for this state.

Two (2 + 1′) excitation spectra of the NH_3 $\tilde{C}'(v_2'=1)$ state obtained at fixed delay times of 0 and 70 ps are shown in Figure 12b and reveal the opposite behavior as observed for the ND_3 $\tilde{C}'(v_2'=3,4,5)$ levels. The peak with maximum intensity in the spectrum obtained at delay 0 ps, corresponding to transitions to low J',K' rotational levels, decreases rapidly in intensity as the delay time is increased, whereas the peak at lower excitation energy, for which the transition to the $J',K' = 6,6$ rotational level is mainly responsible, maintains its intensity up to a delay time of 70 ps. This behavior is in agreement with the results given in Table 4, which show that the rotational levels around $J',K' = 6,6$ in the excited state have lifetimes of about 100 ps, whereas the low J',K' rotational levels have considerably shorter lifetimes of about 25 ps.

III.E. Comparison between Picosecond and Nanosecond Results. In this section the results from the present, real-time, natural lifetime measurements obtained using the picosecond excitation source will be compared to the results obtained with nanosecond excitation in this study as well as in previous studies. From Table 4 we observe that rotational levels with high J',K' associated with the $\tilde{C}'(v_2'=1,2)$ vibrational members of NH_3 have a longer lifetime than rotational levels with low J',K'. The same conclusion has been drawn above from the nanosecond excitation spectra of these states in which the intensities of transitions to rotational levels with high J',K' were found to be larger than expected on the basis of the simulations (see also Figure 5). The long lifetime determined for the NH_3 $\tilde{C}'(v_2'=3)$ state (see Table 4 and Figure 10) would seem to be at odds with the weak and diffuse appearance of this band in the nanosecond excitation spectrum. In the previous sections it was shown, however, that at least one rotational level, presumably the $J',K' = 6,0$ level, appears to have a considerably longer lifetime than the other rotational levels (see Figure 6). If the transition to this level dominates the picosecond excitation spectrum as well, it can be understood that its lifetime of 15 ps dominates the picosecond decay trace, whereas the short lifetimes of the other rotational levels are responsible for the weak and diffuse appearance of the nanosecond excitation spectrum.

The lifetimes of the rotational levels associated with the ND_3 $\tilde{C}'(v_2'=2)$ vibrational state determined by line width measurements in a previous study were shown to depend on the rotational quantum numbers J',K'.[27] The line widths of the individual rotational levels could be modeled by the equation $\omega = \omega_0\{1 + 0.030[J'(J' + 1) - (K')^2]\}$, in which the natural line width of the $(J'',K'' = 0,0) \rightarrow\rightarrow (J',K' = 0,0)$ transition $\omega_0 = 0.012\ cm^{-1}$, corresponding to a natural lifetime of 450 ps of the $(J',K') = (0,0)$ rotational level. This equation shows that the largest changes should occur for the rotational levels for which $K' \ll J'$, such as $J',K' = 7,1$ and that the differences in lifetime for levels with $J' \sim K'$ are only minor. The rotational contour simulations of the $\tilde{C}'(v_2')$ states have shown that transitions to the latter type of rotational levels, *i.e.* $(J'',K'') \rightarrow (J' = J'',K' = K'')$, tend to contribute the most intensity to the excitation spectrum. It can thus qualitatively be understood that we observe no rotational level dependence in the picosecond decay measurements of the ND_3 $\tilde{C}'(v_2'=2)$ vibrational level, whereas such a dependence was concluded from the line width measurements.[27]

Our decay measurements on the higher members of the $\tilde{C}'$ progression in ND_3, *i.e.*, $\tilde{C}'(v_2'=3,4,5)$, clearly show that the higher J',K' rotational levels are shorter lived than the low J',K' levels (see Table 4, Figures 11 and 12). This effect has been observed previously in the (3+1) excitation spectra of ND_3, where it affected the peak heights.[26] The conclusion of earlier studies[26,27,45] that a rotationally dependent predissociation mechanism is operative in the v_2' vibrational members of the $\tilde{C}'$ state in NH_3 and ND_3 is confirmed in the present results. The effect of a second, homogeneous, predissociation mechanism, which has been concluded to be important for the higher $\tilde{C}'(v_2' \geq 3)$ vibrational members in NH_3 on the basis of the nanosecond excitation spectra, is not observed in our picosecond real-time measurements on NH_3 due to the reasons discussed above. In ND_3, however, this homogeneous predissociation mechanism is observed to be responsible for a decrease in the natural lifetime as higher v_2' vibrational levels of the $\tilde{C}'$ Rydberg state are addressed (see Table 4).

For the $\tilde{B}(v_2')$ states of NH_3, Table 4 shows lifetimes of the rotational levels which are on the order of 6.8−9.4 ps and only slightly dependent on v_2', J', and K'. This is in agreement with the peak heights in the nanosecond excitation spectra as well as with the line width measurements in the present study and a previous study on the $\tilde{B}(v_2')$ states by Ashfold *et al.*[29] Similar arguments apply to the $\tilde{B}(v_2')$ states in ND_3, but there is an additional point of interest. In the study of Ashfold *et al.* the line widths of the rotational lines in the $\tilde{B}(v_2'=0-6)$ transitions indicated natural lifetimes of 250 ± 20 ps, independent of v_2', J', and K'. In the line width study evidence was found, however, that the lifetime of the $\tilde{B}(v_2'=8)$ state in ND_3 is substantially shorter than the lifetime of the $\tilde{C}'(v_2'=2)$ state and also shorter than that of the lower v_2' members $(v_2' \leq 6)$ of the $\tilde{B}(v_2')$ progression. We find in our picosecond real-time results lifetimes for the $\tilde{B}(v_2'=8,10)$ vibrational levels of about 75 ps, independent of v_2', J', and K'. Our results are in agreement with the results of Ashfold *et al.* In both studies there appears to be a sudden lowering of the natural lifetime in the $\tilde{B}(v_2')$ progression in ND_3 for $v_2' \geq 8$, which is unexpected in view of the apparent overall independence of the natural lifetimes on v_2'.

The implications of the observed $\tilde{B}(v_2')$ and $\tilde{C}'(v_2')$ predissociation dynamics for the identification of the states responsible for the predissociation process have been discussed by Ashfold *et al.*[26,29] Briefly, the $\tilde{A}\ ^1A_2''$ Rydberg state has been identified as the main cause for the predissociation of the higher-lying Rydberg states: the $\tilde{B}$ and $\tilde{C}'$ Rydberg states are coupled to relatively short-lived rovibronic levels associated with this $\tilde{A}$ state *via* vibronic operators q_i or rovibronic operators $q_iJ_\pm$, of which the latter are expected to give much smaller matrix elements than the former. The present as well as previous results[29] suggest that the predissociation behavior of the rotational levels associated with the $\tilde{B}(v_2')$ vibrational levels is dominated by a coupling *via* the q_3 vibronic operator to dissociative rovibronic levels of the $\tilde{A}\ ^1A_2''$ state. The natural lifetimes of the rotational levels are thus independent of v_2', since the coupling operator does not contain q_2, and also independent of the excited-state rotational quantum numbers J',K', because the coupling operator does not include $J_\pm$. However, the observation that the lifetime of the rotational levels

associated with the $\tilde{B}(v_2')$ states in ND_3 decreases abruptly from about 250 ps for $v_2' = 0-6$ to about 75 ps for $v_2' = 8,10$ finds no explanation within this model. The predissociation dynamics of the rotational levels associated with the $\tilde{C}'(v_2')$ states are determined by two coupling mechanisms which might be equally important. The first coupling mechanism couples $\tilde{C}'(v_2')$ states *via* the $q_3J_\pm$ rovibronic operator to dissociative rovibronic levels of the $\tilde{A}\ ^1A_2''$ state and is responsible for the J',K' dependence of the natural lifetimes of the rotational levels in the $\tilde{C}'$ state. The second coupling mechanism couples $\tilde{C}'(v_2')$ states *via* the q_2 vibronic operator to relatively long lived rovibronic levels in the $\tilde{A}\ ^1A_2''$ state and results in the experimentally observed v_2'-dependent homogeneous predissociation in the $\tilde{C}'(v_2')$ vibrational members.

In a previous section it was shown that the photoelectron spectra obtained *via* the $\tilde{B}(nv_2')$ vibrational members in NH_3 and ND_3 were dominated by electrons corresponding to ions in the $\tilde{X}\ ^2A_2''(nv_2^+)$ state, while weaker electron signals, corresponding to ions in the $\tilde{X}\ ^2A_2''((n\pm1)v_2^+)$ and $\tilde{X}\ ^2A_2''(nv_2^+ + v_4^+)$ states, were identified as well. The appearance of these weak signals is surprising because, within the Born–Oppenheimer approximation, ionization to these vibrational levels in the $\tilde{X}\ ^2A_2''$ ionic ground state should be strictly forbidden. The activity of the v_4^+ vibration could in principle become allowed as a result of the Jahn–Teller effect in the $\tilde{B}$ state.[29,33,39] A tentative alternative explanation may be found in the coupling mechanism of the $\tilde{B}(v_2')$ states to vibronic levels associated with the $\tilde{A}\ ^1A_2''$ Rydberg state. If the $\tilde{B}(v_2')$ states are vibronically coupled to the $\tilde{A}\ ^1A_2''$ states *via* q_4, which on symmetry grounds would be possible, then the photoelectron spectra obtained *via* the $\tilde{B}(v_2')$ states would contain, apart from the $\Delta v_2 = 0$ photoelectron peak, also v_4^+ activity. Similarly, vibronic coupling *via* v_2 would induce v_2^+ activity.

III.F. Fragmentation Mechanisms. The predissociation dynamics of the $\tilde{A}\ ^1A_2''$ Rydberg state of ammonia have been studied extensively in the past.[4,7,10,17–24] Several of these studies have investigated which fragment species are produced and how the excess energy is redistributed among the translational, vibrational, and rotational degrees of freedom of the fragments. Such studies do not exist for the predissociation dynamics of the $\tilde{B}$ and $\tilde{C}'$ Rydberg states, but as the dynamical behavior of these states is believed to be determined to a major extent by the predissociation behavior of the $\tilde{A}$ state, their fragmentation is expected to resemble the $\tilde{A}$ state fragmentation with the important difference that considerably more excess energy is available after fragmentation of the $\tilde{B}$ and $\tilde{C}'$ states. Once a specific rotational level of the $\tilde{B}(^1E'', v_2'$ is even; $^1E', v_2'$ is odd) or $\tilde{C}'(^1A_1', v_2'$ is even; $^1A_2'', v_2'$ is odd) has been excited in a two-photon absorption step, the following competing processes can occur:

$$NH(D)_3\ \tilde{B}(^1E'',^1E'),\ \tilde{C}'(^1A_1',^1A_2'') + h\nu \rightarrow NH(D)_3^+\ \tilde{X}(^2A_2'') + e^- \quad (1)$$

$$NH(D)_3\ \tilde{B}(^1E'',^1E'),\ \tilde{C}'(^1A_1',^1A_2'') \rightarrow NH(D)_2\ \tilde{X}(^2B_1),\ \tilde{A}(^2A_1) + H(D)(1s) \quad (2)$$

$$NH(D)_3\ \tilde{B}(^1E'',^1E'),\ \tilde{C}'(^1A_1',^1A_2'') \rightarrow NH(D)_3\ \tilde{A}(^1A_2'',^1A_1') + h\nu' \quad (3)$$

Up until now we have almost exclusively discussed the ionization process (1) in our experimental results. The predissociation (2) and fluorescence[45,56,57] (3) processes compete with the ionization process. Two-photon excitation spectra of the $\tilde{C}'(v_2'=0,1)$[45] and $\tilde{C}'(v_2'=2)$[57] vibrational levels have been obtained previously by monitoring the strong fluorescence (3) to the $\tilde{A}$ state. As the predissociation channel (2) becomes progressively more important for the states which lie at higher energies, the parent molecule fluorescence disappears and the fluorescence of the $NH(D)_2\ \tilde{A}(^2A_1)$ fragment appears. Even though the quantum yield for this species is only a few percent, its fluorescence has been observed to be modulated by the $\tilde{B}(v_2')$ and $\tilde{C}'(v_2')$ vibrational members.[18,49–51,64]

In the present study only positive ions or electrons can be detected, and in order to observe a neutral predissociation fragment, it needs to be ionized first. The $NH(D)_2\ \tilde{X}(^2B_1)$ fragment has been reported to produce REMPI signals in a previous study,[33] but in the present experiments we have concentrated on the hydrogen atom. If the laser wavelength of the nanosecond dye laser is tuned to 34 275 cm^{-1}, the rotational levels in the wing of the $\tilde{C}'(v_2'=5)$ vibrational level in NH_3, about 100 cm^{-1} lower in energy than the band maximum, are excited in a two-photon absorption process. From this level the molecule can be ionized by process (1) or predissociate by process (2). On predissociation the $H(1s\ ^2S_{1/2})$ atom can subsequently be ionized in a (3 + 1) REMPI process *via* the $4p\ ^2P^o_{1/2,3/2}$, $4f\ ^2F^o_{5/2,7/2}$ levels using the same wavelength with which NH_3 was excited and ionized.[65] Under the experimental conditions where the electrons from the H atom ionization can be observed, the electrons deriving from ionization of the parent molecule produce a signal, which is at least 1 order of magnitude stronger. It is nevertheless possible to observe the electrons deriving from the ionization of the hydrogen atoms. From the Doppler broadening of the corresponding peak in the photoelectron spectrum it can be inferred that the neutral hydrogen atoms obtain a kinetic energy of about 0.3 eV upon predissociation. The same experiment using picosecond excitation failed to produce the electrons deriving from the ionization of the hydrogen atoms. Even in a two-color picosecond experiment, in which the first color was tuned to the (3 + 1) resonance in atomic hydrogen as described above and the second color to the maximum of the $\tilde{C}'(v_2'=5)$ band, neither electrons in the photoelectron time-of-flight spectrum nor ions in the mass-resolved ion spectrum attributable to ionization of atomic hydrogen could be observed. The fact that atomic hydrogen signals are not observed when picosecond excitation is used possibly arises from a less efficient competition of the predissociation mechanism with the parent ionization process within the picosecond excitation pulse.

In a two-color experiment using nanosecond excitation in combination with mass-resolved ion detection, we have monitored the production of hydrogen atoms from the predissociation of the Rydberg states. In these experiments one of the dye lasers is tuned to a wavelength of 41 129.5 cm^{-1}, corresponding to the strong two-photon $1s\ ^2S_{1/2} \rightarrow\rightarrow 2s\ ^2S_{1/2}$ transition of the H atom,[65–67] while the second dye laser is scanned over various v_2' vibrational levels of the $\tilde{B}$ and $\tilde{C}'$ states. In agreement with a previous study we find that the mass-resolved ion spectrum contains only NH_3^+ ions, when only the laser beam which excites the $\tilde{B}(v_2')$ and $\tilde{C}'(v_2')$ vibrational levels is present.[58] When the laser beam which is set at the H atom resonance is present as well, an additional H^+ signal is observed, which disappears completely when either laser beam is blocked. Under optimum experimental conditions for the H^+ signal, the NH_3^+ signal, which results from the (2 + 1) one-color REMPI process, is about 1 order of magnitude larger. The H^+ signal is observed to be modulated by the $\tilde{B}$ and $\tilde{C}'$ resonances. Figure 13 shows the excitation spectrum of the $\tilde{C}'(v_2'=2)$ vibrational level in NH_3 for two competing channels, *viz.*, the ionization channel and

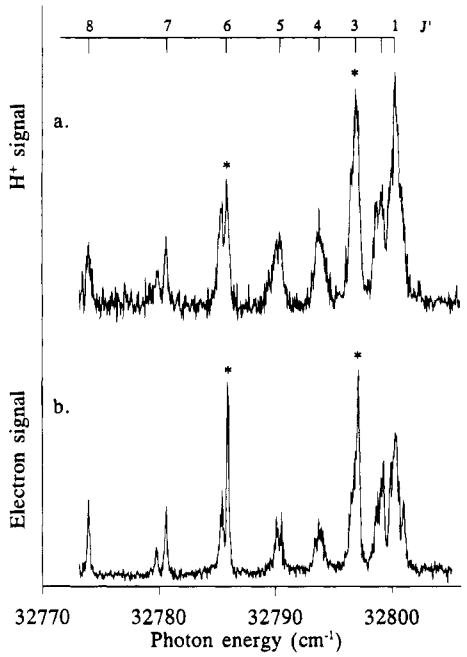

Figure 13. Nanosecond excitation spectra of the $\tilde{C}'(v_2'=2)$ band in NH_3, in which the H^+ ion signal (a) and the electron signal deriving from (2 + 1) ionization of NH_3 (b) are monitored. The peaks labeled with an asterisk are weak in part a and strong in part b. The main progression, attributable to the $(J'',K'') \rightarrow \rightarrow (J',K' = J'',K'')$ transitions, is marked at the top of the figure.

the predissociation channel. In Figure 13b the regular one-color total electron signal is shown, while in Figure 13a the two-color H^+ signal is shown. The strong $(J'',K'') \rightarrow \rightarrow (J',K' = J'',K'')$ progression has been marked at the top of the figure. A number of transitions, indicated in Figure 13 with an asterisk, are relatively strong in Figure 13b and relatively weak in Figure 13a. As before, this suggests that these transitions take place to rotational levels in the excited state which have longer lifetimes with respect to the other rotational levels, resulting in an enhancement of the ionization yield with respect to the predissociation yield. This is in agreement with the other measurements on the $\tilde{C}'(v_2'=2)$ level in the present study, such as the rotational contour simulations and the real-time picosecond natural lifetime measurements.

IV. Conclusions

In the present study we have investigated the dynamical predissociation behavior of the rotational levels associated with the $\tilde{B}(v_2')$ and $\tilde{C}'(v_2')$ Rydberg states in ammonia with (2 + 1) and (2 + 1′) REMPI spectroscopy. The natural lifetimes of these levels have been measured in real time by a combination of picosecond excitation with photoelectron spectroscopy. It has been shown that, with the use of different colors for excitation and ionization, photoelectron spectroscopy provides the opportunity to observe background-free decay traces. The predissociation behavior of the rotational levels associated with the $\tilde{B}(v_2')$ and $\tilde{C}'(v_2')$ states has also been examined with a nanosecond excitation source using indirect methods, such as determination of the natural line widths of the rotational lines and comparison of the intensities of the rotational lines with theoretical rotational contour predictions in the excitation spectra. The results from the direct measurements in the present study using picosecond excitation have been shown to be in excellent agreement with the results from the above indirect methods using nanosecond excitation in both the present work and in previous studies.

The use of high-resolution photoelectron spectroscopy has enabled the identification of all photoelectron peaks in the (2 + 1) REMPI–PES spectra obtained for excitation *via* the $\tilde{B}(v_2')$ vibrational members in NH_3 and ND_3. The vibrational frequencies for the symmetric stretch vibration ν_1 and for the asymmetric bending vibration ν_4 in NH_3^+ (ND_3^+) as determined from these spectra are 0.404 ± 0.007 eV (0.304 ± 0.007 eV) and 0.197 ± 0.007 eV (0.141 ± 0.007 eV).

In a two-color experiment using nanosecond excitation the hydrogen atom, which results from the predissociation process in the $\tilde{B}$ and $\tilde{C}'$ Rydberg states, has been observed. The excitation spectra of the competing predissociation and ionization channels in these Rydberg states agree well with the conclusions obtained from the lifetime measurements.

Acknowledgment. We gratefully acknowledge Professor M. N. R. Ashfold for stimulating discussions, N. P. L. Wales for his assistance during the experiments, Ing D. Bebelaar for technical support, and the Netherlands Organization for Scientific Research (NWO) for equipment grants and financial support.

References and Notes

(1) Papousek, D. *J. Mol. Struct.* **1983**, *100*, 179.
(2) Urban, S.; Papousek, D.; Bester, M.; Yamada, K.; Winnewisser, G.; Guarnieri, A. *J. Mol. Spectrosc.* **1984**, *106*, 29.
(3) Walsh, A. D.; Warsop, P. A. *Trans. Faraday Soc.* **1961**, *57*, 345.
(4) Douglas, A. E. *Discuss. Faraday Soc.* **1963**, *35*, 158.
(5) Vaida, V.; Hess, W.; Roebber, J. L. *J. Phys. Chem.* **1984**, *88*, 3397.
(6) Ziegler, L. D. *J. Chem. Phys.* **1985**, *82*, 664.
(7) Ashfold, M. N. R.; Bennett, C. L.; Dixon, R. N. *Chem. Phys.* **1985**, *93*, 293.
(8) Xie, J.; Bo, J.; Zhang, C.; Sha, G.; Zhang, X. *J. Opt. Soc. Am. B* **1986**, *3*, P134.
(9) Xie, J.; Sha, G.; Zhang, X.; Zhang, C. *Chem. Phys. Lett.* **1986**, *124*, 99.
(10) Ashfold, M. N. R.; Bennett, C. L.; Dixon, R. N. *Faraday Discuss. Chem. Soc.* **1986**, *82*, 163.
(11) Ziegler, L. D. *J. Chem. Phys.* **1987**, *86*, 1703.
(12) Vaida, V.; McCarthy, M. I.; Engelking, P. C.; Rosmus, P.; Werner, H.-J.; Botschwina, P. *J. Chem. Phys.* **1987**, *86*, 6669.
(13) Rosmus, P.; Botschwina, P.; Werner, H.-J.; Vaida, V.; Engelking, P. C.; McCarthy, M. I. *J. Chem. Phys.* **1987**, *86*, 6677.
(14) Engelking, P. C.; Vaida, V. *Int. J. Quantum Chem.* **1987**, *29*, 73.
(15) Chung, Y. C.; Ziegler, L. D. *J. Chem. Phys.* **1988**, *89*, 4692.
(16) Tang, S. L.; Imre, D. G. *Chem. Phys. Lett.* **1988**, *144*, 6.
(17) Runau, R.; Peyerimhoff, S. D.; Buenker, R. J. *J. Mol. Spectrosc.* **1977**, *68*, 253.
(18) Donnelly, V. M.; Baronavski, A. P.; McDonald, J. R. *Chem. Phys.* **1979**, *43*, 271.
(19) McCarthy, M. I.; Rosmus, P.; Werner, H.-J.; Botschwina, P.; Vaida, V. *J. Chem. Phys.* **1987**, *86*, 6693.
(20) Biesner, J.; Schnieder, L.; Schmeer, J.; Ahlers, G.; Xie, X.; Welge, K. H.; Ashfold, M. N. R.; Dixon, R. N. *J. Chem. Phys.* **1988**, *88*, 3607.
(21) Dixon, R. N. *Chem. Phys. Lett.* **1988**, *147*, 377.
(22) Biesner, J.; Schnieder, L.; Ahlers, G.; Xie, X.; Welge, K. H.; Ashfold, M. N. R.; Dixon, R. N. *J. Chem. Phys.* **1989**, *91*, 2901.
(23) Dixon, R. N. *Mol. Phys.* **1989**, *68*, 263.
(24) Woodbridge, E. L.; Ashfold, M. N. R.; Leone, S. R. *J. Chem. Phys.* **1991**, *94*, 4195.
(25) Ziegler, L. D.; Kelly, P. B.; Hudson, B. *J. Chem. Phys.* **1984**, *81*, 6399.
(26) Ashfold, M. N. R.; Dixon, R. N.; Stickland, R. J. *Chem. Phys.* **1984**, *88*, 463.
(27) Ashfold, M. N. R.; Dixon, R. N.; Rosser, K. N.; Stickland, R. J.; Western, C. M. *Chem. Phys.* **1986**, *101*, 467.
(28) Ashfold, M. N. R.; Bennett, C. L.; Stickland, R. J. *Comments At. Mol. Phys.* **1987**, *19*, 181.
(29) Ashfold, M. N. R.; Dixon, R. N.; Little, N.; Stickland, R. J.; Western, C. M. *J. Chem. Phys.* **1988**, *89*, 1754.
(30) Harshbarger, W. R. *J. Chem. Phys.* **1971**, *54*, 2504.
(31) Nieman, G. C.; Colson, S. D. *J. Chem. Phys.* **1978**, *68*, 5656.
(32) Nieman, G. C.; Colson, S. D. *J. Chem. Phys.* **1979**, *71*, 571.
(33) Glownia, J. H.; Riley, S. J.; Colson, S. D.; Nieman, G. C. *J. Chem. Phys.* **1980**, *73*, 4296.
(34) Douglas, A. E.; Hollas, J. M. *Can. J. Phys.* **1961**, *39*, 479.

(35) Stanley, R. J.; Echt, O.; Castleman, A. W., Jr. *Appl. Phys. B* **1983**, *32*, 35.
(36) Conaway, W. E.; Morrison, R. J. S.; Zare, R. N. *Chem. Phys. Lett.* **1985**, *113*, 429.
(37) Kay, B. D.; Grimley, A. J. *Chem. Phys. Lett.* **1986**, *127*, 303.
(38) Kay, B. D.; Raymond, T. D. *Chem. Phys. Lett.* **1986**, *127*, 309.
(39) Ashfold, M. N. R.; Dixon, R. N.; Stickland, R. J.; Western, C. M. *Chem. Phys. Lett.* **1987**, *138*, 201.
(40) Habenicht, W.; Reiser, G.; Müller-Dethlefs, K. *J. Chem. Phys.* **1991**, *95*, 4809.
(41) Glownia, J. H.; Riley, S. J.; Colson, S. D.; Nieman, G. C. *J. Chem. Phys.* **1980**, *72*, 5998.
(42) Nieman, G. C. *J. Chem. Phys.* **1981**, *75*, 584.
(43) Achiba, Y.; Sato, K.; Shobatake, K.; Kimura, K. *J. Chem. Phys.* **1983**, *78*, 5474.
(44) Grimley, A. J.; Kay, B. D. *Chem. Phys. Lett.* **1983**, *98*, 359.
(45) Ashfold, M. N. R.; Bennett, C. L.; Dixon, R. N.; Fielden, P.; Rieley, H.; Stickland, R. J. *J. Mol. Spectrosc.* **1986**, *117*, 216.
(46) Koenders, B. G.; Wieringa, D. M.; Drabe, K. E.; de Lange, C. A. *Chem. Phys.* **1987**, *118*, 113.
(47) Dobber, M. R.; Buma, W. J.; de Lange, C. A. *J. Chem. Phys.* **1993**, *99*, 836.
(48) Dobber, M. R.; Buma, W. J.; de Lange, C. A. *J. Chem. Phys.* **1994**, *101*, 9303.
(49) Okabe, H.; Lenzi, M. *J. Chem. Phys.* **1967**, *47*, 5241.
(50) Quinton, A. M.; Simons, J. P. *J. Chem. Soc., Faraday Trans. 2* **1982**, *78*, 1261.
(51) Suto, M.; Lee, L. C. *J. Chem. Phys.* **1983**, *78*, 4515.
(52) Watson, J. K. G.; Majewski, W. A.; Glownia, J. H. *J. Mol. Spectrosc.* **1986**, *115*, 82.
(53) Herzberg, G. *Molecular Spectra and Molecular Structure II, Infrared and Raman Spectra of Polyatomic Molecules*; Van Nostrand, New York, 1954.
(54) Herzberg, G. *Molecular Spectra and Molecular Structure III, Electronic Spectra and Electronic Structure of Polyatomic Molecules*; Van Nostrand, New York, 1966.
(55) Chen, K.; Yeung, E. S. *J. Chem. Phys.* **1978**, *69*, 43.
(56) Quick, C. R., Jr.; Glownia, J. H.; Tiee, J. J.; Archuleta, F. L. *Proc. SPIE Int. Soc. Opt. Eng.* **1983**, *380*, 156.
(57) Glownia, J. H.; Hartford, A., Jr.; Loge, G. W.; Sander, R. K.; Tiee, J. J.; Wampler, F. B. *Adv. Laser Spectrosc.* **1983**, *2*, 105.
(58) Glownia, J. H.; Riley, S. J.; Colson, S. D.; Miller, J. C.; Compton, R. N. *J. Chem. Phys.* **1982**, *77*, 68.
(59) Pallix, J. B.; Colson, S. D. *J. Phys. Chem.* **1986**, *90*, 1499.
(60) Miller, P. J.; Colson, S. D.; Chupka, W. A. *Chem. Phys. Lett.* **1988**, *145*, 183.
(61) Weiss, M. J.; Lawrence, G. M. *J. Chem. Phys.* **1970**, *53*, 214.
(62) Rabalais, J. W.; Karlsson, L.; Werme, L. O.; Bergmark, T.; Siegbahn, K. *J. Chem. Phys.* **1973**, *58*, 3370.
(63) Locht, R.; Leyh, B.; Denzer, W.; Hagenow, G.; Baumgärtel, H. *Chem. Phys.* **1991**, *155*, 407.
(64) Xuan, C. N.; Di Stefano, G.; Lenzi, M.; Margani, A. *J. Chem. Phys.* **1981**, *74*, 6219.
(65) Moore, C. E. *Atomic Energy Levels*; Natl. Stand. Ref. Data Ser., Natl. Bur. Stand. 35; U.S. GPO: Washington, DC, 1971; Vol. 1.
(66) Bjorklund, G. C.; Ausschnitt, C. P.; Freeman, R. R.; Storz, R. H. *Appl. Phys. Lett.* **1978**, *33*, 54.
(67) Ausschnitt, C. P.; Bjorklund, G. C.; Freeman, R. R. *Appl. Phys. Lett.* **1978**, *33*, 851.
(68) Jacox, M. E. *J. Phys. Chem. Ref. Data* **1988**, *17*, 269.

JP941639Q